PLM: EFFICIENT PERIPHERAL LANGUAGE MODELS HARDWARE-CO-DESIGNED FOR UBIQUITOUS COMPUTING

Cheng Deng^{1,*,†}, Luoyang Sun^{2,*}, Jiwen Jiang^{2,*}, Yongcheng Zeng², Xinjian Wu³, Wenxin Zhao¹, Qingfa Xiao¹, Jiachuan Wang⁴, Haoyang Li⁵, Lei Chen^{1,4}, Lionel M. Ni¹, Haifeng Zhang², Jun Wang^{3,6,†}

¹The Hong Kong University of Science and Technology (Guangzhou)

²Institution of Automation, Chinese Academy of Sciences

³University College London

⁴The Hong Kong University of Science and Technology

⁵The Hong Kong Polytechnic University

⁶UCL Centre for Artificial Intelligence
davendw49@gmail.com, leichen@cse.ust.hk, jun.wang@cs.ucl.ac.uk

PLM Team

https://github.com/plm-team/PLM

ABSTRACT

While scaling laws have been continuously validated in large language models (LLMs) with increasing model parameters, the inherent tension between the inference demands of LLMs and the limited resources of edge devices poses a critical challenge to the development of edge intelligence. Recently, numerous small language models have emerged, aiming to distill the capabilities of LLMs into smaller footprints. However, these models often retain the fundamental architectural principles of their larger counterparts, still imposing considerable strain on the storage and bandwidth capacities of edge devices. In this paper, we introduce the PLM, a Peripheral Language Model, developed through a co-design process that jointly optimizes model architecture and edge system constraints. The PLM utilizes a Multi-head Latent Attention mechanism and employs the squared ReLU activation function to encourage sparsity, thereby reducing peak memory footprint during inference. During training, we collect and reorganize open-source datasets, implement a multi-phase training strategy, and empirically investigate the Warmup-Stable-Decay-Constant (WSDC) learning rate scheduler. Additionally, we incorporate Reinforcement Learning from Human Feedback (RLHF) by adopting the ARIES preference learning approach. Following a two-phase SFT process, this method yields performance gains of 2% in general tasks, 9% in the GSM8K task, and 11% in coding tasks. In addition to its novel architecture, evaluation results demonstrate that PLM outperforms existing small language models trained on publicly available data while maintaining the lowest number of activated parameters. Furthermore, deployment across various edge devices, including consumer-grade GPUs, mobile phones, and Raspberry Pis, validates PLM's suitability for peripheral applications. The PLM series models, including PLM-1.8B-Base and PLM-1.8B-Instruct, are publicly available at https://github.com/plm-team/PLM.

1 Introduction

Large Language Models (LLMs) have revolutionized various AI applications. On-device LLMs are gaining prominence, as running these models locally on edge devices can avoid the drawbacks brought by the cloud-based LLMs, like

^{*}Equal contribution.

[†]Correspondence to Cheng Deng, Lei Chen, Jun Wang.

[‡]Version: v1 (major update on 15th March, 2025).









Figure 1: System hardwares used in our experiments: (L-R) Broadcom (Raspberry Pi), NVIDIA Jetson Orin NX, Apple M3 (MacBook Air 2024), Qualcomm Snapdragon 8 Gen 3 (OnePlus 12 Pro), and the NVIDIA A10 experimental device is installed in the server.

privacy risks from uploading sensitive data [1], increased carbon footprint due to data transfers and reliance on cloud GPUs [2], and inaccessibility during network outages, limiting use in critical applications [3]. In many specialized fields, applying AI is challenging due to the trade-off between model size [4] and available computing resources.

To address this concern, Small Language Models (SLMs) have emerged as a viable solution [5]. The 1.5B models in the Qwen series [6, 7] exemplify out-of-the-box LLMs optimized for small-scale deployment. Similarly, the MiniCPM series [8] demonstrates the potential of end-side LLMs, while the SmolLM [9] and Yulan-mini [10] series provide compelling evidence that high-quality training data significantly enhances the performance of SLMs. Moreover, Deepseek has put forward a reasoning model based on Qwen2-1.5B distilled from Deepseek R1 [11], making it a direction for making SLM have the abilities of reasoning and doing decision.

Beyond training models at a reduced scale, model compression techniques such as AWQ [12] and GPTQ [13] offer alternative approaches to facilitate LLM deployment in resource-constrained environments. Moreover, advancements in inference methods have been closely aligned with system constraints, enabling efficient deployment. For instance, MLC-LLM [14], leveraging the TVM backend [15], along with frameworks such as llama.cpp [16] and PowerInfer [17, 18], enable optimized performance on various edge CPU and GPU platforms. Additionally, systems like vLLM [19] and SGLang [20] provide significant acceleration on devices with limited computational resources.

The research and development efforts in this domain consistently highlight the constraints of computing resources on edge devices, underscoring the critical challenge of peripheral computing. In practical scenarios, such as on mobile phones and personal computers, available memory cannot be exclusively allocated to LLMs. During real-world deployment, computational resources must be shared with other applications. This challenge becomes even more pronounced on specialized System-on-Chip (SoC) platforms, such as personal computer, mobile phone, and Raspberry Pi devices. These scenarios necessitate dynamic resource management, where the model is loaded into memory only when required and its occupied memory is released when no longer in use.

PowerInfer2 [18] and LLM in the Flash [21] offer promising solutions to address these challenges. However, the inference process of LLMs introduces additional complexity, as the generation of KV caches increases both computational demands and memory usage. Offloading KV caches to external storage mitigates memory constraints but simultaneously incurs higher I/O overhead, thereby imposing additional limitations on many deployment scenarios.

What constitutes the most effective model design for edge devices? There is no universally accepted answer to this question. Based on extensive research and experimental validation, in this paper, we shares the way we think, design, train and deploy the LLM on edge devices.

Current advancements in LLM design highlight two critical components for optimization: attention mechanisms and MLP layers. Attention mechanisms often represent a significant computational bottleneck during LLM inference, particularly as sequence lengths increase. Innovations in attention design provide valuable solutions to this challenge. MLP layers play a critical role in processing each token independently to refine its representation through dense matrix multiplications and activation functions. However, these operations contribute significantly to the computational load in LLMs.

Our proposed model, PLM (Peripheral Language Model), builds upon the strengths of recent advancements by achieving a balance between performance and efficiency. Guided by the principle of modeling and system co-design, PLM incorporates innovative features such as squared ReLU, an activation function inspired by recent research of activation sparsity in LLMs [22, 23, 24], designed to enhance computational sparsity. Additionally, PLM leverages Multi-Head Latent Attention (MLA) [25], incorporating insights from Deepseek-v2 from the angle of low-rank to achieve superior efficiency in attention mechanisms.

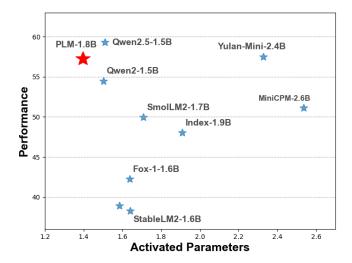


Figure 2: Evaluations on LLM benchmarks demonstrate that our sparsified MLA models, PLM, maintain competitive performance. The performance is evidenced by the averaged benchmark scores in section 5, in terms of general knowledge comprehension (MMLU, CMMLU, C-Eval, ARC), Math problem solving (GSM8K and MathQA), coding proficiency (HumanEval and MBPP), and commonsense and logical reasoning (HellaSwag, BooQ, LogiQA, and PIQA). Meanwhile, the activated parameters are determined by the minimal computation required to preserve modeling performance. Detailed results are presented in section 7.

In this report, we introduce PLM, a series of edge-oriented LLMs that address key research challenges, including sketching model architecture through language modeling and system co-design, multi-phases training using Warm-up-Stable-Decay-Constant (WSDC) learning rate scheduler, multi-phases supervised fine-tuning from shallow to deep, preference learning, and fast inference on peripheral devices. To support further research and application development, we publicly release PLM model weights. The distinctiveness and contributions of PLM can be summarized as follows:

- 1. Introducing PLM-1.8B, a novel LLM tailored for peripheral devices. This 1.8 billion-parameter model leverages multi-head latent attention and a squared ReLU sparsification technique. It demonstrates competitive performance against similarly sized LLMs trained on open-source data, while also providing efficient decoding capabilities.
- 2. In this report, we detail the whole construction progress of PLM, including modeling, data curation, sandbox experiments, training, model evaluation, and deployment on edge devices.
- 3. We discuss the observation and benefit of PLM. Utilizing the "low-rank and sparsity" modeling and system co-design, we implement the examples on edge devices, such as consume level GPUs, Jetson Orin, mobile phone, personal laptop, and Raspberry Pis.
- 4. We discuss the key factors in the LLM design for peripheral computing, from the perspective of peripheral systems and language modeling co-design. Based on the methods survey and observation from the benchmarking experiments, we illustrate the future development of the edge LLM for peripheral computing and beyond.

All the models, data used, benchmarks, and related introduction are shown on Github and https://sites.google.com/view/project-plm.

2 Architecture

Number of	Hidden	Number of	Number of	KV LoRA	Sequence	Intermediate	Vocabulary	Attention	Activation
layers	Dimension	Attention Heads	KV Heads	Rank	Length	Size	Size	Type	Function
32	2,048	16	16	512	4,096	8,192	151,936	MLA	${ m ReLU^2}$

Table 1: Core settings decide the size of PLM-1.8B.

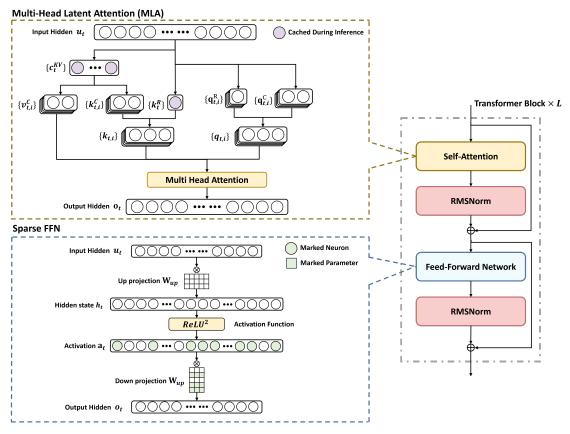


Figure 3: PLM architecture.

PLM is based on a standard decoder-only Transformer architecture. Specific hyperparameters related to model size are provided in Table 1. The model consists of 0.31B embedding parameters and 1.51B non-embedding parameters. Key architectural features include Multi-head Latent Attention (MLA) [25], Decoupled Rotary Position Embeddings (RoPE) [26], a BPE tokenizer inheriting the Qwen2 tokenizer [6], squared ReLU activations [24] within the MLP layers, and tied input-output embeddings.

Multi-head Latent Attention (MLA) [25] We use MLA in PLM, which is an advanced architectural enhancement designed to improve the efficiency of LLMs by significantly reducing the memory footprint associated with key-value (KV) caching. Conventional multi-head attention mechanisms maintain independent key and value vectors for each attention head, leading to substantial memory consumption. In contrast, MLA employs low-rank matrix decomposition to compress these projections into a shared latent space of reduced dimensionality. This approach enables the model to store a compact representation while reconstructing the necessary vectors dynamically during computation, thereby preserving model performance while substantially lowering memory overhead.

By alleviating memory bottlenecks and improving scalability, MLA enhances the feasibility of deploying LLMs in resource-constrained environments, particularly on edge devices where lightweight, scalable, and computationally efficient models are required to deliver real-time performance. To further optimize PLM, we adapt the original MLA framework by omitting compression on the query projections within the attention mechanism.

In the context of processing the attention input for the t-th token within an attention layer, MLA introduces Low-Rank Key-Value $Joint\ Compression$ by applying a down-projection to the token's hidden state h_t , formulated as:

$$\boldsymbol{c}_{t}^{KV} = W_{DKV}\boldsymbol{h}_{t},\tag{1}$$

where c_t^{KV} represents the latent embedding of the keys and values, and W_{DKV} denotes the down-projection matrix. The key and value representations for the *i*-th attention head are subsequently reconstructed using the up-projection matrices $W_{UK,i}$ and $W_{UV,i}$, while the query is computed separately using the matrix $W_{Q,i}$:

$$\mathbf{k}_{t,i}^{C} = W_{UK,i} \mathbf{c}_{t,i}^{KV}, \quad \mathbf{v}_{t,i}^{C} = W_{UV,i} \mathbf{c}_{t,i}^{KV}, \quad \mathbf{q}_{t,i}^{C} = W_{Q,i} \mathbf{h}_{t}.$$
 (2)

Notably, we deliberately refrains from applying low-rank compression to the queries. While query compression can enhance training efficiency, it introduces additional computational overhead during inference, which is undesirable in latency-sensitive applications. Finally, we integrate the Decoupled Rotary Position Embedding (RoPE) mechanism to further refine the attention dynamics. In summary, PLM leverages MLA with preserving the full-rank structure of the query projections to balance training efficiency and inference speed effectively.

Sparse FFN We adopt a streamlined Feed-Forward Network (FFN) architecture that omits gating mechanisms, thereby reducing computational complexity and memory usage. To further enhance efficiency, *ReLU*² activations [24] is an activation function that achieves an optimal trade-off between performance and sparsity, making it highly advantageous for sparse computation in practice. Defined as follows:

$$ReLU^{2}(x) = (\max(0, x))^{2} = \begin{cases} x^{2}, & \text{if } x > 0, \\ 0, & \text{if } x \leq 0. \end{cases}$$
 (3)

ReLU² introduces quadratic growth in activation values, enabling the network to capture richer feature representations. ReLU² demonstrates exceptional performance by balancing sparsity and computational efficiency, allowing models to dynamically skip inactive neurons while maintaining high accuracy. Furthermore, ReLU² enhances hardware affinity by consistently activating similar neurons across consecutive tokens, effectively reducing the I/O overhead in feedforward networks.

With the combination of a low-rank attention mechanism and sparse activation function integration, we balance KV cache reduction and computational load across the model, achieving a trade-off between memory cost and latency. Briefly, PLM used squared ReLU without hidden state gating.

In our investigation, the use of MLA in MiniCPM3 [8] and the adoption of ReLU² activations in Nemotron-4 [27], and related empirical study [28] provided compelling evidence supporting this combination strategy. Furthermore, we conducted a series of architecture search experiments, with a particular focus on the relationship between the number of attention heads and the hidden dimension, driven by our implementation of MLA. These insights were instrumental in finalizing the architecture of the PLM model.

3 Data

Compared to the well-established data engineering and accumulation approaches in industry, we employ high-quality open-source datasets alongside research-oriented strategies for data collection and generation. Specifically, we construct chain-of-thought reasoning data, augment data using Retrieval-Augmented Generation (RAG), and distill data from large-parameter language models. We then train PLM in three distinct phases: (1) stable learning of general knowledge, (2) integration of high-quality data, and (3) learning on internal, knowledge-intensive datasets. This three-phase approach yields a comprehensive training corpus for PLM.

3.1 Data Collection

Open-source Dataset Collection Following the recommendations of recent surveys [29, 30], we select open-source datasets based on three key principles: high quality, large volume, and coverage of various domains. A detailed list of the pre-training datasets is provided in subsection B.1. To filter these datasets, we employ the data classifier offered by CCI3-HQ. Specifically, we utilize texts annotated with scores from DCLM and CCI3-HQ, perform score normalization, and train a scoring model. This scoring model is then applied to datasets lacking intrinsic scoring or quality metrics (e.g., MAP-cc), enabling us to sample data according to the assigned scores. Furthermore, we use the MinHash algorithm, as recommended by the Data-Prep-Kit [31], to remove duplicate entries from the Chinese training corpus. Due to the limited time and data processing efficiency, we pose a room for the improvement in the next version of PLM.

Synthetic Data Construction Synthetic data generation has become an increasingly important tool for LLM research and development [32]. It mitigates data shortages, helps reduce biases, ensures compliance with privacy regulations, and steers models toward more specialized or robust capabilities. Inspired by Cosmopedia [33] and the use of extended Chain-of-Thought reasoning [34, 35], we generate an internal dataset for pre-training PLM.

3.2 Data for Pre-Training

In the first phase, we train PLM on a pre-training dataset comprising 1.65 trillion tokens in total. The dataset spans four main categories—English, Chinese, Code, and Mathematics. The English dataset (DCLM) is split evenly into five subsets, each containing 280B tokens. The Chinese dataset includes CCI3-HQ (180B), MAP-CC (high-quality; 120B), and MAP-CC (medium-quality; 400B). The Code dataset is derived entirely from StarCoder (230B). Finally, the Mathematics dataset combines Proof-Pile (58B) and MathPile (12B), resulting in a comprehensive training corpus. Detailed configurations of these datasets for Phase 1 are shown in Table 19.

Table 2: Summary of training data distribution and allocation of phase 1.

Category	Data Source	Selected Size (B)	Training Allocation (B)	Normalized Ratio
English	DCLM	1485	966	58.3%
Chinese	CCI3-HQ, MAP-CC	648	483	29.2%
Code	StarCoder	226	158	9.6%
Math	Proof-Pile, MathPile	59	48	2.9%

In the second phase, we train PLM on a higher-quality dataset totaling 550B tokens, encompassing Chinese general data, English general data, and additional content (e.g., code and math) at a 5:2:2 ratio. The Chinese dataset is downsampled such that the Chinese Fineweb Edu component is reduced to 120B tokens, while the remaining datasets are weighted according to their respective token counts.

During this phase, we also introduce high-quality instruction data, including extended Chain-of-Thought (CoT) data produced by the OpenR [35] framework (0.009B), QA data (0.12B), and Zh_Baike (0.019B) generated using GPT4o. The primary sources in this phase comprise Chinese Fineweb Edu v2 (120B), the SmolLM Corpus (222B), and the YuLan-Mini-Datasets (65B). Within the SmolLM Corpus, Cosmopedia-v2 (27.2B), FineWeb-Edu (191.4B), and Python-Edu (3.4B) are included. The YuLan-Mini-Datasets encompass deduplicated Python data (36B) and synthetic code, math, and QA data (29B).

Furthermore, we incorporate the Opc-annealing-corpus (64B) and Dolmino-mix-1124 (74B), the latter containing Flan data (17B) and the Pes2o academic paper dataset (60B). Detailed dataset compositions and specifications for Phase 2 are provided in Table 3.

Table 3: Summary of training data distribution and allocation of phase 2.

Category	Data Source	Selected Size (B)	Training Allocation (B)	Normalized Ratio
English	SmolLM-Corpus, dolmino-mix-1124-Flan	292.6	300	54.5%
Chinese	Chinese-Fineweb-Edu-V2	221	120	21.8%
Math, Code, Paper	opc-annealing-corpus, dolmino-mix-1124-pes2o, YuLan-Mini-Datasets	132.4	130	23.6%

During Phase 3, we curated a smaller but more diverse dataset to further refine the model's capabilities. In this phase, we utilized an Internal Instruction-Restructured Dataset, detailed in subsection B.2) to improve instruction-following performance and alignment with downstream tasks, with over 60M samples. For advanced reasoning, we leveraged the high-value YuLan-Mini-Dataset and selected the corrsponding part. We also incorporated Dolmino-Mix-1124-Math, a high-quality math-related dataset.

To maintain general knowledge, we selectively down-sampled datasets such as FineWeb-Edu from SmolLM-Corpus and Chinese-FineWeb-Edu-V2, an upgraded version. This comprehensive and strategically refined dataset supports the development of an LLM with broad versatility and strong domain-specific expertise. The distribution are summarized in Table 4

Table 4: Summary of training data distribution and allocation of phase 3.

Category	Data Source	Selected Size (B)	Training Allocation (B)	Normalized Ratio
English	SmolLM-Corpus	191	95.2	34.0%
Chinese	Chinese-Fineweb-Edu-V2	221	38.1	13.6%
Math, Code, Paper	YuLan-Mini-Datasets, dolmino-mix-1124-math	108	101.9	36.4%
Instruction-Restructured	Internal Dataset	47	44.8	16.0%

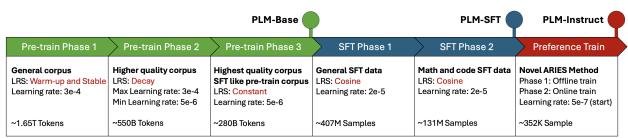


Figure 4: Training pipeline adapted for PLM.

3.3 Data for Post-Training

During the post-training phase, we employ open-source *instruction—input—output* triplet datasets to perform supervised fine-tuning on PLM, enhancing its ability to follow instructions and generate high-quality responses. Additionally, we incorporate both offline and online preference data to conduct reinforcement learning with human feedback, further refining PLM's performance.

Supervised Fine-tuning Data Following the systematic data preparation approach used in K2 [36], we structure the supervised fine-tuning process in a progressive manner. The training of PLM is conducted in two distinct phases:

- Phase 1 (Basic Instruction Tuning): In the initial phase, we utilize 17 general-domain instruction tuning datasets, comprising a total of 407M samples. These datasets are sourced from publicly available internet corpora or distilled from larger, more capable models. Notably, some datasets contain coding- and math-related tasks, which we retain as they contribute to enhancing the model's reasoning capabilities.
- Phase 2 (Advanced Instruction Tuning): In the second phase, we incorporate 30 datasets, a total of 131M samples, including three trust-and-safety datasets, ten mathematical datasets, six coding datasets, and ten high-quality, knowledge-intensive instruction tuning datasets. A subset of datasets from Phase 1 is retained to maintain distributional balance within the training data. The inclusion of specialized datasets in this phase aims to further improve the model's competency in complex reasoning and domain-specific tasks.

RLHF Data During the reinforcement learning stages, our objective is to align PLM with human expression preferences while preserving its performance across various benchmarks. To achieve this, we first conduct offline fine-tuning of PLM utilizing the llama-3.1-tulu-3-70b-preference-mixture general preference dataset ¹ [37]. Following this, we employ the prompt dataset from Ultrafeedback ² [38] to gather on policy data. Combining this with the CodeUltraFeedback dataset ³ [39], we then perform a second round of preference training on PLM. This approach ensures that the model effectively adapts to human-like response preferences without compromising its overall task performance.

The details of the supervised fine-tuning data are shown in section B.3. Moreover, it is important to note that PLM is exclusively trained on Chinese (Simplified) and English instruction corpora and alignment corpora, filtered using Langid ⁴ to ensure linguistic consistency.

4 Pre-Training Details

The PLM pre-training process consists of three core elements: search and selection of an appropriate model architecture, the stage of pre-training, and the stage of post-training. This section provides a detailed illustration of each sessions.

4.1 Model Architecture Search

Since PLM uses MLA as the attention mechanism, and the ReLU² as the activation function at the same time, and PLM is designed for peripheral scenarios, we do sandbox experiments for search the best model architecture. Since we target the edge devices, we observe the theoretical amount of floating-point operations (FLOPs), multiply-add operations

https://huggingface.co/datasets/allenai/llama-3.1-tulu-3-70b-preference-mixture

 $^{^2} https://huggingface.co/datasets/HuggingFaceH4/ultrafeedback_binarized$

³https://huggingface.co/datasets/coseal/CodeUltraFeedback_binarized

⁴https://github.com/saffsd/langid.py

(MACs), and the empirical performance on 100B specially-selected dataset sampled from the final pre-train corpus. The selected experimented architectures and the results are shown as follows.

#Params 5	$ n_{layer} $	d_{model}	d_{ffn}	kv_{rank}	MACs/Param	FLOPs/Param	Time/Layer	Peak Memory	Loss
1.54B	28	2816	7040	256	0.5243	1.261e-4	7.3188	7.031e-5	2.639
1.21B	32	2304	5760	256	0.2023	5.209e-4	3.2364	7.578e-5	2.653
1.47B	32	2560	6400	256	0.1986	3.660e-4	3.1728	6.595e-5	2.659
1.36B	36	2304	5760	256	0.1806	4.142e-4	3.2660	6.802e-5	2.653
1.51B	40	2304	5760	256	0.1645	3.365e-4	3.2853	7.121e-5	2.665

3.512e-4

4.214e-4

7.184e-5

6.687e-5

2.632

2.634

3.2225

2.7499

0.1785

0.1722

Table 5: Experiments for architecture search, Appendix A records more experimental results and details.

4.2 Pre-training

36

32

2048

2048

8192

8192

256

512

1.55B

1.54B

We train PLM on a total of **2.48 trillion tokens**. Refer to [8], during the training, we deploy a WSDC learning rate scheduler, adding one more phase with constant learning rate after the stage of decay, which proceeds in three phases:

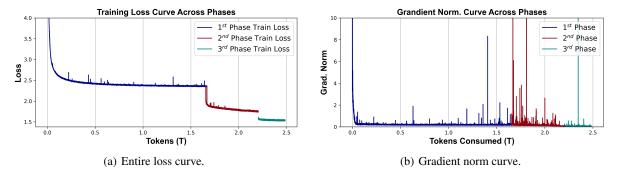


Figure 5: Pre-training loss curve for PLM.

- **Phase 1 (Warm-up and Stable)**: For 1% of the total steps, the learning rate gradually increases until it reaches a peak of *3e-4*, which is then maintained.
- Phase 2 (Decay): The learning rate is reduced to 3e-5 while the model shifts to smaller, higher-quality datasets.
- **Phase 3 (Constant)**: During the final phase of pre-training, spanning the last 280 million tokens, we utilize a Constant learning rate, maintaining a context length of 4,096 tokens. In this phase, we introduced instruction-like data and significantly up-sampled the high-quality data from phase 2.

Throughout training, we maintained a fixed sequence length of 4K tokens and utilized a batch size of 15 million tokens, distributed across 208 accelerators. The training curves for PLM-1.8B-Base are presented in Figure 6. The details of the pre-training are introduced in subsection C.1.

During phase 1 of training, we continuously monitored the validation loss to evaluate the model's performance. Following the methodology outlined in [40], we estimated PLM's performance throughout training and reported its improvements alongside the total number of tokens processed.

As illustrated in 6(a), the model converged to a validation loss exceeding 2.3 (The majority of emergent abilities manifest when the training loss is below 2.2 [40]). Given the constraints of the initial dataset, we opted to incorporate a higher-quality dataset for subsequent training phases, as suggested in [41].

Building on these WSD stages, we extended pre-training to enhance the model's expertise in mathematics, coding, and encyclopedic knowledge, thereby boosting its performance on knowledge-intensive tasks.

During the phase 3, inspired by the training strategies of ResNet [42], we adjusted the learning rate to 3e-5 and initiated a cosine decay learning rate schedule. This adjustment guided the training process through an additional 280 billion tokens, culminating in the final stage of model optimization.

⁵It is refers to non-embedding parameters here.

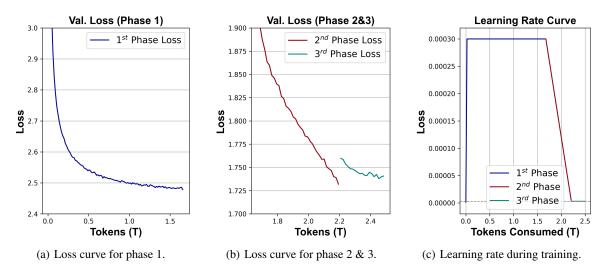


Figure 6: Phase level pre-training loss curve for PLM.

4.3 Supervised Fine-tuning

In the the stage of supervised fine-tuning, we refer to both data-centric model training [36] and empirical learning on SFT and RL [43], we deploy a two-phase training in a progressive manner. For each phase we utilize LLaMA-Factory [44] to do full-parameter SFT over prepared datasets. The detail training arguments are shown in subsection C.2.

During the training, in Phase 1, we utilize a diverse range of general-purpose instruction-following datasets, including those focused on chat, web questions, and general instruction. In Phase 2, we expand upon this with a significant emphasis on specialized domains, particularly mathematics and coding, incorporating datasets designed for complex reasoning, code generation, and domain-specific instruction following in areas like education and medicine. This progression suggests a strategy of initially building a strong foundation in general capabilities before refining the model's expertise in specialized tasks.

Finally, we obtain the PLM-Instruct, and the Figure 7 shows the curves during this two phases SFT training.

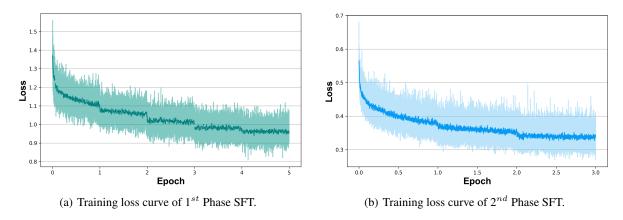


Figure 7: SFT training curve for PLM.

4.4 Preference Training

Previous open-source LLMs have exhibited a significant limitation: their performance often degrades markedly after multiple rounds of self-refinement. This behavior is inconsistent with the expected characteristics of highly intelligent language models. To address this issue, during the preference training phase, we adopt a novel training approach akin

to our method, ARIES [45]. We leverage ARIES' self-refinement loss to conduct preference training on PLM:

$$\mathcal{L}_{\text{ARIES}}(\pi_{\theta}; \pi_{\text{ref}}) = (1 - \alpha)\mathcal{L}_{\text{DPO}}(\pi_{\theta}; \pi_{\text{ref}}) + \alpha\mathcal{L}_{\text{refine}}(\pi_{\theta}; \pi_{\text{ref}}), \tag{4}$$

where the refinement loss is employed to stimulate and strengthen the model's self-refinement capability:

$$\mathcal{L}_{\text{refine}}(\pi_{\theta}; \pi_{\text{ref}}) = \underset{(x, y_w, y_l) \sim \mathcal{D}}{\mathbb{E}} \left[\frac{1}{2} - \beta \left[\log \left(\frac{\pi_{\theta}(y_w | x, y_l, z)}{\pi_{\text{ref}}(y_w | x, y_l, z)} \right) - \log \left(\frac{\pi_{\theta}(y_l | x, y_l, z)}{\pi_{\text{ref}}(y_l | x, y_l, z)} \right) \right] \right]^2 + \underset{(x, y_w, y_l) \sim \mathcal{D}}{\mathbb{E}} \left[\frac{1}{2} - \beta \left[\log \left(\frac{\pi_{\theta}(y_w | x, y_w, z)}{\pi_{\text{ref}}(y_w | x, y_w, z)} \right) - \log \left(\frac{\pi_{\theta}(y_l | x, y_w, z)}{\pi_{\text{ref}}(y_l | x, y_w, z)} \right) \right] \right]^2.$$
(5)

In the above loss function, x denotes the input prompt, y_w is the chosen response, y_l is the rejected response, and $\mathcal{D} = \{(x^{(i)}, y_w^{(i)}, y_l^{(i)})\}_{i=1}^N$ represents the preference dataset, z denotes the refinement template, while π_{ref} and π_{θ} represent the reference model and the learnable policy model, respectively. The parameter β controls the strength of the regularization term, which penalizes deviations from the reference model π_{ref} . This loss function also demonstrates an auxiliary effect in improving the model's direct answering ability in experiments.

The overall training pipeline for preference training follows a similar approach to ARIES. We first conduct an offline preference training round on the llama-3.1-tulu-3-70b-preference-mixture dataset ⁶ [37] (**Phase 1**), and then sample 5K prompt dataset from the UltraFeedback dataset ⁷ [38] to gather on policy dataset. Combining this with the CodeUltraFeedback preference dataset ⁸ [39], we perform a second round of preference training on PLM (**Phase 2**). During the data collection process, we employ the RLHFlow/ArmoRM-Llama3-8B-v0.1 ⁹ [46] as the reward model to construct the preference dataset. The basic argument settings and training curves are shown in subsection C.3.

5 Evaluation: Training Results

As an LLM tailored for edge-based peripheral computing, we first show the results of the training results of PLM, then we perform a comprehensive evaluation from three distinct perspectives: fundamental model performance, architectural efficiency, and real-world operational efficiency. For each aspect, we select appropriate baseline models for comparison. Specifically, for performance evaluation, we rely on quantitative results obtained directly from system feedback.

5.1 Evaluation and Experiment Setup

To evaluate the model trained during the process, assess the effectiveness of the proposed methods, and compare them with baseline models, we conduct a comprehensive evaluation of the LLM's performance. To ensure a thorough assessment, we select benchmarks based on the following aspects.

- Language Modeling: We utilize the subset of DCLM, MAP-cc, StarCoder, and ProofPile, to evaluate the improvement along with the PLM training.
- General Knowledge Comprehension: We utilize widely-adopted benchmarks such as the Massive Multitask Language Understanding (MMLU), Chinese Massive Multitask Language Understanding (CMMLU), Chinese Evaluation (C-Eval), and the AI2 Reasoning Challenge (ARC), which includes both the ARC-Easy (ARC-E) and ARC-Challenge (ARC-C) sets.
- Mathematical Problem Solving: To assess mathematical reasoning, we employ benchmarks like the Grade School Math 8K (GSM8K) and MathQA datasets.
- Coding Proficiency: We evaluate coding capabilities using the HumanEval and Mostly Basic Python Problems (MBPP) benchmarks.
- Commonsense and Logical Reasoning: The model's ability to understand and apply everyday commonsense knowledge is tested using datasets such as HellaSwag, BoolQ, LogiQA, and the Physical Interaction: Question Answering (PIQA) benchmark.

These benchmarks provide a diverse and rigorous framework to assess the model's performance across multiple dimensions. For fair evaluation and comparison in equal, we set *zero-shot* for HumanEval, MBPP, BoolQ, LogiQA, and PIQA, set MMLU, CMMLU, C-Eval, MathQA, and WinoGrande as *5-shots* tasks, HellaSwag as *10-shots* task, and

 $^{^6}$ https://huggingface.co/datasets/allenai/llama-3.1-tulu-3-70b-preference-mixture

 $^{^7 {}m https://huggingface.co/datasets/HuggingFaceH4/ultrafeedback_binarized}$

 $^{^8}$ https://huggingface.co/datasets/coseal/CodeUltraFeedback_binarized

⁹https://huggingface.co/RLHFlow/ArmoRM-Llama3-8B-v0.1

ARC-e and ARC-e as 25-shots tasks. For evaluation consistency, we use EvalPlus [47] for the evaluation of Coding Proficiency, and utilize the LM-Evaluation Harness [48] to assess the performance of PLM and all the models across the rest of aforementioned tasks.

5.2 Evaluating Model Performance during Training

In this section, we summarize the key findings from the phased training and evaluation of PLM, integrating insights from the provided perplexity measurements and benchmark results across pre-training, supervised fine-tuning (SFT), and reinforcement learning (RL) stages.

Phased Pre-Training Analysis As shown in Table 6, perplexity consistently decreased across all training corpora (DCLM, MAP-cc, StarCoder, ProofPile) through the three-phase curriculum pre-training. Phase 3 achieved the lowest perplexity (e.g., 6.75 for ProofPile), indicating progressive improvements in the model's ability to predict token sequences across diverse domains. This reduction reflects effective knowledge consolidation, particularly for code and mathematical reasoning tasks, where StarCoder and ProofPile saw substantial gains.

Phase	DCLM	MAP-cc	StarCoder	ProofPile
Phase 1	15.59	11.47	3.13	7.60
Phase 2	14.71	10.54	2.91	7.16
Phase 3	14.61	10.47	2.89	6.75

Table 6: Perplexity observation during the three-phases pre-training.

Supervised Fine-Tuning Results During the SFT stage, we mainly focus on the performance on MMLU, CMMLU, BoolQ, GSM8K, and HumanEval. Table 7 highlights performance gains during SFT. While the base model (PLM-Base) achieved an average score of 51.29 across benchmarks, phased SFT yielded incremental improvements. Notably:

- Phase 2 SFT achieved the highest average score (57.00), with significant gains in reasoning tasks: GSM8K improved by 26 points (34.80 → 60.80) compared to earlier phases, and HumanEval (code generation) rose from 43.30 to 57.90
- Mathematical reasoning (MathQA) and language understanding (BoolQ, ARC-c) also improved, though MBPP (code) saw a temporary dip in Phase 1, recovering in later phases. This suggests task-specific sensitivity to curriculum ordering.

Model	Avg.	MMLU	CMMLU	ARC-c	ARC-e	BoolQ	GSM8K	MathQA	HumanEval	MBPP
PLM-Base	51.29	48.02	45.40	48.12	77.31	73.67	41.70	28.81	43.30	55.30
PLM-SFT-Tulu	51.49	47.67	45.16	48.63	78.24	73.79	34.80	28.71	54.90	54.50
PLM-SFT-Phase-1	52.22	48.99	46.45	51.54	79.00	76.70	35.86	29.55	52.40	49.50
PLM-SFT-Phase-2	57.00	49.79	46.86	49.57	77.98	76.97	60.80	32.53	57.90	60.60

Table 7: SFT results of each phase.

Reinforcement Learning Enhancements After SFT, Our novel RL methods, ARIES [45], further refined performance (Table 8):

- Online RLHF and PLM-Instruct achieved the best overall averages (55.99 and 56.94, respectively), with GSM8K reaching 63.50 (up 5.4 points from SFT) and HumanEval stabilizing at 64.63.
- Identity RL underperformed compared to Online/Offline RLHF, emphasizing the importance of preference-based alignment. Notably, while most tasks improved, MathQA showed minimal gains, indicating limitations in arithmetic generalization.

In general, the phased training curriculum—combining progressive pre-training, task-focused SFT, and preference-aware RLHF enable PLM to achieve robust performance across reasoning, coding, and language understanding benchmarks. Key gains in GSM8K and HumanEval highlight strengths in mathematical and code generation tasks, while fluctuations in MBPP and MathQA suggest avenues for future refinement. These results underscore the efficacy of curriculum-driven training and strategic alignment for specialized capabilities.

	Avg	MMLU	C-Eval	ARC-c	ARC-e	BoolQ	GSM8K	MathQA	HumanEval	MBPP
PLM-1.8B-SFT	56.66	49.79	43.76	49.57	77.98	76.97	60.80	32.53	57.90	60.60
PLM _{Identity RL}	56.78	49.80	44.50	50.43	77.99	74.04	57.16	32.86	64.00	60.30
PLM _{Offline RLHF}	57.51	50.08	43.83	50.94	77.78	77.16	60.73	32.63	64.60	59.80
PLM _{Online RLHF}	58.42	50.47	44.76	52.65	78.68	77.67	63.50	33.11	64.63	60.32

Table 8: Reinforcement learning result of each iteration.

5.3 Evaluating PLM and the baselines

To compare the performance comprehensively, we introduce several small size LLMs with comparable scales to PLM (Under 2.7B, including embedding sizes) as baselines for comparison, we choose three data-close-source models and four data-open-source models, which are listing as follows.

Model	Data	Size	n_{layer}	d_{model}	n_{head}	Attention	Activation	Institute
MiniCPM-2.7B	Close (1.3T)	2.74B	40	2304	36	GQA	SwiGLU	ModelBest
Yulan-Mini-2.4B	Open (1.1T)	2.42B	56	1920	30	GQA	SwiGLU	RUC
Index-1.9B	Open (2.8T)	1.91B	36	2048	16	GQA	SwiGLU	Bilibili
SmolLM2-1.7B	Open (11T)	1.71B	24	2048	32	GQA	SwiGLU	Hugging face
StableLM2-1.6B	Open (2T)	1.64B	24	2048	32	MHA	SwiGLU	StableAI
Fox-1-1.6B	Open (3T)	1.61B	32	2048	32	GQA	SwiGLU	TensorOpera
GLM-Edge-1.5B	Close (-)	1.59B	28	2048	16	GQA	SwiGLU	Zhipu
Qwen2.5-1.5B	Close (18T)	1.54B	28	1536	12	GQA	SwiGLU	Alibaba
Qwen2-1.5B	Close (7T)	1.54B	28	1536	12	GQA	SwiGLU	Alibaba
PLM-1.8B	Open (2.5T)	1.83B	32	2048	16	MLA	ReLU ²	PLM-Team

Table 9: Basic information of the selected baselines.

- Qwen2-1.5B & Qwen2.5-1.5B [6, 7]: We introduce the Qwen series models, particularly Qwen2-1.5B, pre-trained on 7T tokens, and Qwen2.5-1.5B, pre-trained on 18T tokens. These models exhibit strong performance in both general-purpose and domain-specific tasks, although detailed training methodologies remain undisclosed.
- MiniCPM-2.4B [8]: MiniCPM-2.4B, pre-trained on 1.06T tokens, employs an annealing training strategy. Despite its relatively modest parameter count, it delivers impressive performance across general tasks and is optimized for deployment on resource-constrained hardware.
- **GLM-Edge-1.5B** [49]: Released by GLM team, GLM-Edge-1.5B is designed to address the challenges of deploying real-world applications on edge devices. It offers several models in different sizes tailored for natural language multimodal understanding. However, the training data and details are not open-sourced.
- Fox-1-1.6B [50]: Developed by TensorOpera, Fox-1-1.6B is pre-trained on 3T tokens of web-scraped document data using an innovative three-stage data curriculum training strategy.
- Index-1.9B [51]: Developed by Bilibili, Index-1.9B is a lightweight version of the Index models, featuring the base model—which leads benchmarks with 1.9 billion non-embedding parameters and a 2.8T Chinese-English corpus, Index-1.9B has two version, one is trained on the open-sourced corpus named with "pure", and the other is trained over an close-sourced dataset, named "base". We choose Index-1.9B-base as the baseline.
- StableLM2-1.6B [52]: Proposed by StabilityAI, StableLM2-1.6B leverages a blend of open-source datasets for pre-training. Its data selection process is informed by insights from smaller language models to optimize dataset composition.
- SmolLM2-1.7B [9]: Developed by Hugging Face TB Research, SmolLM2-1.7B is pre-trained on an 11T-token high-quality corpus. It achieves a fine balance between computational efficiency and task performance.
- Yulan-Mini-2.4B [10]: Yulan-Mini, our concurrent work, is an exceptional SLM trained on 1.08T tokens sourced entirely from open data. Yulan-Mini stands out for providing complete transparency regarding its development details and training corpus.

As shown in Table 10, PLM performs competitively, securing the third-highest average score (57.29), just behind Qwen2.5-1.5B (59.25) and Yulan-Mini-2.4B (57.51). Notably, PLM-1.8B achieves the highest score in HumanEval among all models and ranks second in ARC-C, ARC-E, MBPP, and BoolQ, slightly trailing the industry-leading Qwen2.5-1.5B. This highlights its strong general knowledge comprehension and coding capabilities.

Compared to Qwen2.5-1.5B, PLM-1.8B falls slightly behind in general knowledge benchmarks such as MMLU, CMMLU, and C-Eval, though its strong performance in ARC-E demonstrates its competency in reasoning tasks. However, it is worth noting that the Qwen series leverages an 18T closed-source corpus. Against Yulan-Mini-2.4B, PLM-1.8B performs slightly worse in coding and logical reasoning tasks but remains a competitive option overall. Furthermore, with only 1.8B parameters and fewer layers (32 (PLM) vs 56 (Yulan-Mini)), PLM would offer significantly lower inference latency.

In conclusion, PLM-1.8B is a strong and reliable model, particularly in basic knowledge understanding, coding and simple reasoning tasks. Appendix F shows the cases generated by PLM.

Benchmark	MiniCPM 2.7B	Yulan-Mini 2.4B	Index 1.9B	SmolLM2 1.7B	Fox 1.6B	StableLM2 1.6B	Qwen2.5 1.5B	Qwen2 1.5B	GLM-Edge 1.5B	$\begin{array}{c} PLM_{Base} \\ 1.8B \end{array}$	PLM_{Inst} 1.8B.
ARC-C	43.86	50.51	42.23	50.29	41.21	40.78	53.41	43.90	24.15	48.12	51.14
ARC-E	55.51	69.87	67.05	77.78	65.00	54.00	79.13	62.21	36.83	77.31	78.18
MMLU	51.13	49.10	50.98	51.91	43.05	40.37	59.79	56.50	54.84	48.02	51.18
CMMLU	48.97	48.35	53.79	33.46	28.28	29.29	67.82	70.30	54.23	45.40	48.18
C-Eval	48.24	51.47	54.82	35.10	28.75	26.99	69.05	70.60	55.05	44.50	44.93
GSM8K	53.83	66.65	28.66	47.68	36.39	20.62	68.50	46.90	54.89	41.70	60.73
MathQA	30.59	34.84	31.79	34.30	27.30	21.56	35.14	31.66	33.94	28.81	33.23
HumanEval	50.00	61.60	1.20	23.35	24.57	8.50	37.20	34.80	1.21	43.30	64.60
MBPP	47.31	66.70	33.07	45.00	16.54	17.50	60.20	46.90	3.44	55.30	60.40
BoolQ	73.55	70.89	83.24	72.26	71.93	69.08	72.91	72.69	60.95	73.67	77.86
Hellaswag	53.06	71.47	70.91	71.48	62.32	67.79	67.73	65.41	29.39	66.27	68.17
LogiQA	31.64	29.65	30.41	29.65	28.57	27.19	31.03	31.02	22.73	29.19	30.12
PIQA	77.04	76.50	76.11	77.04	75.35	74.10	76.01	<u>75.35</u>	74.32	75.35	76.01
Average	51.13	57.51 (2 nd)	48.02	49.95	42.25	38.29	59.84 (1 st)	54.48	38.92	52.07	57.29 (3 rd)

Table 10: Comparison between and other representative models.

6 Evaluation: In the Context of Modeling-Hardware Co-Design

In this section, we introduce the baseline models from the perspectives of modeling-hardware co-design and architectural comparisons during inference. This analysis provides insights into the trade-offs between efficiency and performance across different model designs.

- MiniCPM Series [8], we choose 2.7B model and 4B model developed by ModelBest, models designed for edge-devices. Moreover, the 4B parameter model also incorporates the MLA mechanism.
- **GLM-Edge** (1.5B and 4B) [49]: Released by GLM team, GLM-Edge-1.5B is designed to address the challenges of deploying real-world applications on edge devices. It offers several models in different sizes tailored for natural language multimodal understanding. However, the training data and details are not open-sourced.
- **Nemotron** [53], a 4B parameter model released by NVIDIA, employing the squared ReLU (ReLU²) activation function to enhance expressivity and computational efficiency.
- Fox [50], a 1.6B parameter model developed by TensorOpera, which leverages Grouped-Query Attention (GQA) and the SwiGLU activation function. Given that Fox is a 32-layer dense model, we consider it a direct baseline for efficiency comparisons.
- Index [51], a 1.9B parameter model developed by Bilibili, utilizing Multi-Query Attention (MQA) alongside the SwiGLU activation function.

These models employ diverse attention mechanisms and activation functions, each optimized for different computational constraints and inference efficiency requirements. In our evaluation of model efficiency, on one hand, Nemotron-4B and GLM-Edge-4B are treated as a comparative group. A comparison between MiniCPM-4B and GLM-Edge-4B illustrates the inference speed impact of MLA, while a comparison involving Nemotron-4B and GLM-Edge-4B demonstrates the speed benefits of sparsity. In a separate comparison, PLM-1.8B, Fox-1.6B, Index-1.9B, and GLM-Edge-1.5B are analyzed as a group. A direct speed comparison between Fox-1.6B and PLM-1.8B highlights the differences between our model design and prevalent architectures at equivalent layer counts. The impact of layer count on inference speed is demonstrated by comparing Fox-1.6B and GLM-Edge-1.5B. Lastly, the difference in model size between Index-1.9B and PLM-1.8B highlights the impact of size on small language model performance.

By analyzing their performance characteristics and design rationales, we aim to systematically assess the impact of modeling and system co-design on efficiency and scalability.

Model	Attention	Activation	Parameters
MiniCPM3-4B	MLA	SwiGLU	4.21B
GLM-Edge-4B	GQA	SwiGLU	4.21B
Nemotron-4B	GQA	$ReLU^2$	4.13B
MiniCPM2	MLA	SwiGLU	2.74B
GLM-Edge-1.5B	GQA	SwiGLU	1.59B
Fox-1.6B	GQA	SwiGLU	1.67B
Index-1.9B	MQA	SwiGLU	1.91B
PLM-1.8B	MLA	$ReLU^2$	1.83B

Table 11: Baseline models compared in edge-side practice evaluation.

Furthermore, we evaluate the performance of deploying models on different kinds of hardware, including consumer level GPU (NVIDIA A10), edge-side GPU (Jetson), CPU (Intel CPU), Hybird process unit (Apple M3 and Qualcomm Snapdragon 8 Gen 3) and entry-level ARM SoC process unit (Broadcom BCM2712). Particularly, we evaluate the selected architectures with the most representative models, shown in Table 11.

- **NVIDIA A10**, based on the Ampere architecture, features 24 GB of GDDR6 memory, a 150W TDP, and is optimized for AI inferencing, training, VDI, and visualization in enterprise workloads. We use single A10 chip to present general edge-side GPU setting.
- **Jetson Orin NX 16GB**, based on NVIDIA's Ampere architecture, features an 8-core Cortex-A78AE CPU, a 1024-core Ampere GPU with 32 Tensor Cores, 16 GB of LPDDR5 memory (102.4 GB/s), and delivers up to 100 TOPS for edge AI and robotics applications. We use single A10 chip to present edge-side high-performance computing unit setting.
- Apple M3, a 3nm SoC, features an 8-core CPU (4P + 4E), up to 10-core GPU with ray tracing, a 16-core Neural Engine (18 TOPS), and supports up to 24 GB LPDDR5 memory (100 GB/s), powering MacBooks and iMacs. We use MacBook Air M3 in the experiments.
- Qualcomm Snapdragon 8 Gen 3, built on a 4nm process, features an 8-core CPU (1 Cortex-X4, 3 Cortex-A720 @ 3.15 GHz, 2 Cortex-A720 @ 2.96 GHz, 2 Cortex-A520), an Adreno 750 GPU, LPDDR5X support (24 GB, 76.8 GB/s), and advanced AI and imaging capabilities. We use the One Plus 12 as the experiment environment.
- **Broadcom BCM2712** is an entry-level ARM SoC featuring a quad-core Cortex-A76 CPU, VideoCore V3D VII GPU (12 cores, 800 MHz), LPDDR4X memory (32-bit, 17 GB/s), and H.264 1080p60 decode/1080p30 encode. Used in the Raspberry Pi 5, it is built on a 16nm process.

Table 12 presents a comprehensive evaluation of inference latency for various edge-size LLMs across different hardware platforms and quantization levels. The models assessed include GLM-Edge-4B, Nemotron, MiniCPM3, MiniCPM2, GLM-Edge-15B, PLM (bold), Fox, and Index, with activation functions such as SwiGLU and ReLU² under varying attention mechanisms. Latency measurements are provided for both prefill (512 tokens) and generation (128 tokens) scenarios, comparing full-precision (FP16) and lower-bit quantizations (Q8, Q4). The results span multiple computing platforms, including high-performance GPUs (NVIDIA A10, Orin NX), Apple's M3 chip, Qualcomm's Snapdragon 8 Gen 3, and embedded systems like BCM2712.

The data reveal significant trade-offs between precision and efficiency, with quantized models (Q8, Q4) generally offering lower memory cost compared to their FP16 counterparts, particularly suitable for edge devices. However, the extent of latency reduction varies by model architecture and hardware, with Snapdragon 8 Gen 3 and M3 achieving competitive performance in specific settings. This analysis highlights the importance of selecting appropriate quantization strategies and hardware acceleration for balancing model performance and computational efficiency in real-world deployment scenarios.

In general, PLM demonstrates strong optimization for both FP16 and quantized configurations (8-bit and 4-bit), positioning it as a highly efficient model for inference across diverse hardware platforms. Notably, PLM surpasses Fox on the Snapdragon 8 Gen 3 in both the FP16 generation case and the 8-bit quantization prefill case (underline), despite having the same number of layers and leveraging a widely deployed architecture. This performance advantage suggests that PLM is particularly well-suited for latency-sensitive applications, offering significant benefits for real-time inference and on-device LLM deployments where computational efficiency is critical. Moreover, Figure 8 visualize the performance and efficiency trade-off of the models.

Table 12: Inference latency of LLMs on various hardware and quantization Levels.

			A10	NVIDIA Orin NX	M3	Snapdragon 8 Gen 3	BCM2712
			0 00 4 00 0		And tombers and forthers	Snapdragon	
							8
			o o o o o o			8	
						Gens	Compute Module[5] 26 0
		GLM-Edge-4B	4335.31 ± 15.52	421.43 ± 15.03	292.84 ± 12.02	12.15 ± 0.15	10.12 ± 0.13
		Nemotron-4B	6543.59 ± 14.38	605.89 ± 12.51	365.06 ± 81.42	20.06 ± 2.29	16.82 ± 0.09
		MiniCPM3-4B MiniCPM-2.7B	3139.28 ± 73.67 6003.20 ± 33.99	331.36 ± 12.91 641.36 ± 10.80	129.27 ± 21.09 488.45 ± 0.61	12.87 ± 1.67 22.09 ± 3.47	4.73 ± 0.45
	Prefill 512	GLM-Edge-1.5B	10074.07 ± 53.99	1217.45 ± 9.74	905.82 ± 0.43	45.33 ± 5.78	17.36 ± 0.08 27.01 ± 0.11
		PLM-1.8B	9129.39 ± 82.80	987.22 ± 19.13	716.94 ± 13.62	44.35 ± 2.11	26.29 ± 1.01
		Fox-1.6B	11616.08 ± 134.66	1351.74 ± 22.89	1032.83 ± 1.50	56.29 ± 2.09	37.80 ± 0.09
FP16		Index-1.9B	8074.48 ± 55.85	488.89 ± 20.53	237.80 ± 3.17	3.62 ± 0.38	23.44 ± 0.02
1110		GLM-Edge-4B	52.25 ± 0.07	6.75 ± 0.04	10.44 ± 0.11	3.34 ± 0.05	0.74 ± 0.01
		Nemotron-4B	63.96 ± 0.08	8.19 ± 0.05	9.01 ± 0.53	4.02 ± 0.08	1.49 ± 0.00
		MiniCPM3-4B	44.17 ± 0.11	5.79 ± 0.01	6.37 ± 1.14	3.16 ± 0.22	0.02 ± 0.00
	Generate 128	MiniCPM-2.7B	72.56 ± 0.17	9.11 ± 0.07	16.31 ± 0.11	4.81 ± 0.19	1.83 ± 0.04
		GLM-Edge-1.5B	131.71 ± 0.26	17.41 ± 0.02	29.57 ± 0.08	11.31 ± 0.62	3.12 ± 0.02
		PLM-1.8B Fox-1.6B	102.30 ± 0.25 117.69 ± 0.26	12.94 ± 0.10 14.90 ± 0.07	23.31 ± 0.05 25.81 ± 0.33	$\frac{10.34 \pm 0.47}{9.07 \pm 1.23}$	2.76 ± 0.00 2.96 ± 0.08
		Index-1.9B	97.36 ± 0.21	14.90 ± 0.07 12.23 ± 0.06	2.22 ± 0.11	9.07 ± 1.23 2.35 ± 0.09	2.40 ± 0.08 2.40 ± 0.00
	<u> </u>	·	<u> </u>				
		GLM-Edge-4B Nemotron-4B	3770.60 ± 7.56 6430.92 ± 29.40	458.50 ± 10.29 728.69 ± 2.00	281.71 ± 8.48 403.62 ± 15.96	18.77 ± 0.13 28.25 ± 0.48	11.37 ± 0.01 17.20 ± 0.11
	Prefill 512	MiniCPM3-4B	3107.81 ± 62.28	349.60 ±4.89	268.59 ± 0.94	17.51 ± 0.16	10.89 ± 0.01
		MiniCPM-2.7B	5279.70 ± 12.02	654.74 ±4.96	463.40 ± 0.52	29.40 ± 0.99	17.96 ± 0.09
		GLM-Edge-1.5B	9030.11 ± 73.89	1156.42 ± 1.56	861.27 ± 0.58	68.36 ± 1.87	30.82 ± 0.03
		PLM-1.8B	8833.31 ± 243.13	989.01 ±3.96	707.76 ± 0.38	64.18 ± 2.51	29.04 ± 0.21
		Fox-1.6B	11250.68 ± 109.62	1385.81 ±17.66	828.30 ± 20.52	58.33 ± 4.20	35.34 ± 4.22
Q8		Index-1.9B	7869.27 ± 37.52	956.54 ± 1.27	581.14 ± 5.25	43.90 ± 0.26	19.93 ± 0.13
		GLM-Edge-4B	83.11 ± 0.16	11.79 ± 0.09	19.45 ± 0.03	5.85 ± 0.57	1.18 ± 0.09
		Nemotron-4B	110.29 ± 0.25	14.35 ± 0.16	22.93 ± 0.34	7.79 ± 1.24	2.97 ± 0.00
		MiniCPM3-4B	67.19 ± 0.27	8.61 ± 0.03	17.76 ± 0.10	5.41 ± 0.48	2.38 ± 0.00
	Generate 128	MiniCPM-2.7B	108.06 ± 0.28	14.09 ± 0.05	27.05 ± 0.21	9.06 ± 1.53	3.47 ± 0.01
		GLM-Edge-1.5B PLM-1.8B	191.80 ± 0.40 157.35 ± 0.50	27.43 ± 0.25 20.94 ± 0.19	50.40 ± 0.06 38.89 ± 0.83	17.08 ± 0.35 13.78 ± 0.75	6.19 ± 0.12 5.31 \pm 0.01
		Fox-1.6B	180.39 ± 0.73	23.50 t 0.31	62.00 ± 3.17	15.80 ± 0.73 15.80 ± 1.67	6.00 ± 0.00
		Index-1.9B	152.79 ± 0.38	20.23 ± 0.03	34.46 ± 0.71	13.30 ± 0.55	3.90 ± 0.01
		GLM-Edge-4B	3748.14 ± 11.02	435.25 ± 0.52	293.26 ± 1.39	16.33 ± 0.06	9.187 ± 0.13
		Nemotron-4B	6156.83 ± 5.16	671.07 ± 6.06	376.61 ± 4.36	26.98 ± 0.65	14.03 ± 0.02
		MiniCPM3-4B	2985.06 ± 49.51	332.56±1.63	252.20 ± 4.95	17.08 ± 1.01	9.21 ± 0.01
	Prefill 512	MiniCPM-2.7B	5291.98 ± 10.21	614.94 ± 3.27	445.00 ± 1.16	24.56 ± 0.18	14.88 ± 0.13
	1101111 312	GLM-Edge-1.5B	8929.26 ± 102.41	1062.21 ± 0.48	826.42 ± 0.57	61.93 ± 1.83	23.61 ± 0.02
		PLM-1.8B	8266.53 ± 209.05	910.61 ± 6.02	680.78 ± 0.33	48.05 ± 7.07	23.57 ± 0.18
		Fox-1.6B Index-1.9B	$10483.37 \pm 69.05 7443.99 \pm 46.19$	1284.18 ±16.86 858.28 ± 4.56	789.35 ± 6.44	58.19 ± 0.27 40.06 ± 1.41	31.42 ± 0.32
Q4					532.56 ± 81.38		19.61 ± 0.13
		GLM-Edge-4B	118.08 ± 0.25	16.63 ± 0.05	31.12 ± 0.08	7.40 ± 1.07	1.98 ± 0.01
		Nemotron-4B	145.60 ± 0.55	18.34 ± 0.15	34.61 ± 1.04	10.54 ± 0.13	4.54 ± 0.01
		MiniCPM3-4B MiniCPM-2.7B	85.33 ± 0.33 145.41 ± 0.37	12.00 ± 0.07 19.37 ± 0.13	26.67 ± 0.15 40.84 ± 0.06	5.46 ± 2.58 11.38 ± 0.16	3.92 ± 0.00 5.61 ± 0.02
	Generate 128	GLM-Edge-1.5B	145.41 ± 0.37 255.52 ± 0.94	19.37 ± 0.13 37.88 ± 0.36	40.84 ± 0.06 77.98 ± 0.11	11.38 ± 0.16 24.96 ± 2.08	3.61 ± 0.02 4.54 ± 0.01
		PLM-1.8B	197.48 ± 1.08	27.04 ± 0.12	59.44 ± 0.15	18.74 ± 1.26	8.02 ± 0.03
		Fox-1.6B	226.85 ± 1.00	30.20 ± 0.09	63.66 ± 1.09	17.67 ± 0.93	8.77 ± 0.02
		Index-1.9B	201.02 ± 0.75	26.93 ± 0.17	56.05 ± 0.74	14.66 ± 0.62	7.65 ± 0.03
	·	1	1				

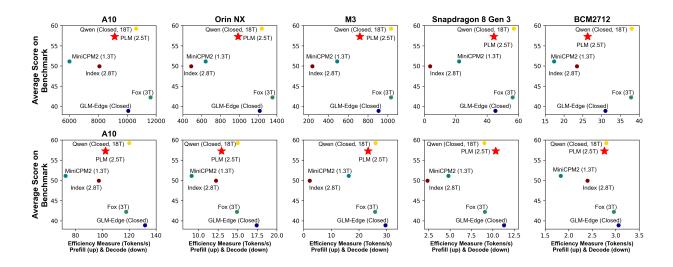


Figure 8: Efficiency comparison of LLMs across different hardware configurations and quantization levels. Optimal hardware-quantization combinations are highlighted, illustrating that PLM achieves an effective balance between robust performance and high inference speed.

7 Analysis: Insights into the Design of PLM

In this section, we will delve into a detailed observation of PLM, aiming to uncover its capabilities, potential, and optimal integration into diverse environments. By addressing two pivotal questions—how to select suitable peripheral language models and the untapped potential of PLM in ubiquitous computing—we provide insights into leveraging PLM for innovative solutions and maximizing its utility across computing paradigms.

7.1 Learned the Attention in PLM

Deploying models on edge devices involves challenges such as limited computational resources, memory capacity, and stringent latency requirements. While Multi-Head Latent Attention (MLA) incurs higher computational overhead than traditional multi-head attention (MHA) and Global Query Attention (GQA), its optimized cache utilization and inference efficiency make it particularly suited for edge deployment.

As shown in Equation 6, the number of KV heads directly impacts the size of the KV cache:

$$Cache_{gqa} = n_{layers} \times 2 \times n_{kv_heads} \times d_h \times \left(\frac{bit \ width}{8}\right) \times N, \tag{6}$$

where n_{layers} is the number of layers, $n_{\text{kv_heads}}$ is the number of KV heads, and d_{h} is the dimensionality of each attention head. The factor of 2 accounts for storing both keys and values and N is the number of token.

However, MLA reduces memory consumption by minimizing KV cache usage, as shown in Equation 7, making it more suitable for memory-constrained edge devices. While MLA incurs higher computational overhead in the prefill phase, this compute-intensive phase benefits from hardware optimizations commonly available on edge devices.

$$Cache_{mla} = n_{layers} \times (d_{rope} + d_c) \times \left(\frac{bit \ width}{8}\right) \times N, \tag{7}$$

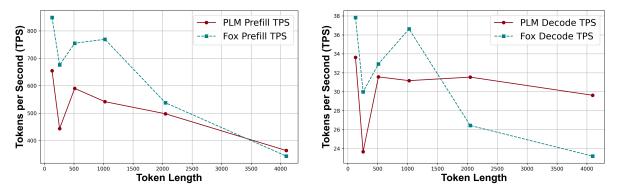
where d_{rope} and d_{c} represent the dimensionalities of the rope key and compressed KV.

While MLA exhibits increased computational demands during prefill, hardware acceleration available on modern edge processors effectively mitigates this cost. The differential decoding complexity between GQA and MLA is sequence-length dependent, scaling as $\mathcal{O}((0.5+2d_c)dN)$, with the cache difference quantified as $\mathcal{O}((2n_{\text{kv_heads}}d_h-d_c-d_{\text{rope}})N)$. Critically, when I/O latency becomes the dominant factor, MLA outperforms GQA. For a detailed analysis of computational costs and cache requirements, refer to Appendix D.

The primary advantage of MLA is evident during the decode phase, which is typically I/O-intensive. MLA reduces memory I/O transfer time by minimizing cache requirements, leading to faster generation despite a slight increase in computational cost. This reduction in I/O time is critical for edge devices, which demand low-latency inference.

In edge inference, quantization further enhances MLA's benefits. After quantization, the reduction in cache usage is linear, while the nonlinear nature of multiplication computations means that additional computational overhead is minimal, further improving memory I/O efficiency. This allows MLA to meet real-time inference demands on edge devices.

Furthermore, MLA minimizes memory consumption by sharing latent spaces across attention heads, reducing cache requirements per head. This is crucial for edge devices, where limited memory impacts system stability and responsiveness. By reducing memory usage, MLA improves performance, particularly in real-time or multi-task inference scenarios.



(a) Effect of token length on tokens per second (TPS) when (b) Effect of token length on tokens per second (TPS) when model prefill.

Figure 9: Effect of token length (PLM vs Fox).

We can anticipate that, in practical exploration, our model will exhibit advantages in certain specialized scenarios due to variations in I/O performance and computational power across different hardware devices. Based on previous experiments, it is evident that Snapdragon demonstrates superior adaptability, outperforming the GQA model Fox of the same depth to some extent, as shown in Table 12. Additionally, we evaluated our model's performance on slightly longer text sequences Figure 9 and identified the advantages of MLA. Compared to DeepSeek's memory-efficient approach on cloud servers, which allows for larger tensor parallelism (TP), we found that MLA maintains its advantages even in edge computing environments where TP is less critical.

Table 13: Latency comparison using 512-tokens prompt to generate 128 tokens and only load each layer iteratively on NVIDIA A10.

Models	Prefill(token/s)↑	Decode(token/s) ↑
PLM-Q8	8237.30	86.19
Fox-Q8	9673.17	67.82
PLM-Q4	7592.33	114.12
Fox-Q4	8888.73	84.21

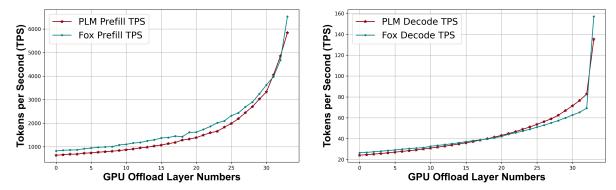
Thus, despite the increased computational load, MLA's optimization of cache utilization, inference efficiency, and memory consumption enables significant advantages for edge devices, offering efficient, low-latency performance in practical applications.

7.2 Learned the Sparsity in PLM

Compared to MLA, the sparsification design of PLM demonstrates more universally effective performance in edge-side models. From a system perspective, or more specifically, from the perspective of computational unit implementation within operating systems, computations involving zeros are highly optimized. Consequently, sparsification significantly benefits the deployment of models on edge devices.

As previously discussed, the introduction of MLA leads to a substantial increase in computational workload. However, by discarding low-rank compression of queries to reduce computational complexity during inference and incorporating sparse activation functions, our model avoids the efficiency drawbacks observed in MiniCPM3 [8], whether in the prefill or decode stages.

In many edge computing scenarios, models often cannot be fully loaded into GPU memory or system RAM, necessitating offloading [21]. Under these conditions, it is crucial to minimize the computational workload for each portion of the model being loaded. Given that deep learning models rely on stacked hidden layers for search and inference, the computational burden at each layer is particularly critical. PLM mitigates this issue by leveraging KV cache storage and sparse activations to reduce computational overhead. Empirically, we set up an experiment to support the opinion shown in Table 13 and Figure 10.



(a) Effect of GPU offload layer number on tokens per second (b) Effect of GPU offload layer number on tokens per second (TPS) when model prefill. (TPS) when model decode.

Figure 10: Effect of GPU offload layer number (PLM vs Fox).

Experimental results validate this advantage. Specifically, when configuring **llama.cpp** to load and infer only one layer at a time, we observed clear benefits from PLM's design, highlighting its efficiency in resource-constrained environments.

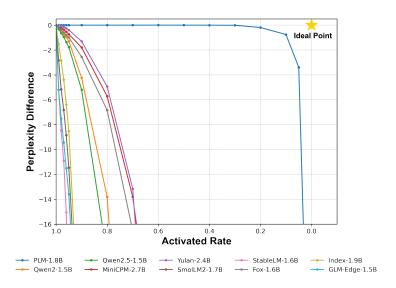


Figure 11: Perplexity increment along with pushing the model to sparse by masking the activated parameters.

Moreover, we study the effective of pushing the model to sparsity. Refer to [22], we design an algorithm to study the sparsity in different baselines. As shown in the Appendix E, the pusedo code of the experiments is Algorithm 1, we calculate and determine the activation sparsity rate in an MLP layer of an LLM, using NVIDIA A10. It first computes the activation output—optionally incorporating a gating mechanism—and establishes a baseline perplexity from a

benchmark dataset. The algorithm then iteratively masks out the smallest r% of activation values (based on their absolute magnitude) and recalculates the model's perplexity by taking the exponential of the negative log likelihood. If masking at a particular sparsity level results in a perplexity reduction of at least I, that r% is identified as the activation sparsity rate. Otherwise, it concludes that no tested sparsity rate meets the desired condition.

More specifically, Figure 11 presents the impact of sparsity on model perplexity. We plotted the difference in perplexity between sparse and dense models against the sparsity rate (ranging from 0 to 1). This allows us to observe the performance cost associated with increasing neural deactivation. The distinct curves for various models reveal the sensitivity of each architecture to sparsity. Notably, the theoretical "ideal point", that full sparsity with no perplexity increase, represents an unattainable goal, where the MLP layer could be completely deactivated without any loss in model quality.

Thus, we can determine the number of parameters actively involved in computation within a model after passing through the activation layer of the MLP. If the computed value is zero, considering it from a hardware perspective, multiplication by zero can be optimized for acceleration. Consequently, from this standpoint, PLM exhibits a significant advantage. As illustrated in the statistics, the sparsity rate of PLM reaches 90.9% in MLP, and 74.3% in total.

On the other hand, we can also analyze this from another perspective, by evaluating the sparsity-induced activation in the MLP, we can quantify the reduction in computational load. As shown in the Table 14, PLM more clearly demonstrates the impact of sparse activation on the overall parameter utilization in this scenario.

Models	Raw Size	Score ↑	Activation Sparsity Rate ¹	Masked Parameters [↑]	Excuted Parameters	Sparsity Rate
MiniCPM-2.6B	2.74	51.13	0.0700	0.0743	2.5357	0.9715
Yulan-Mini-2.4B	2.42	59.25	0.0900	0.0929	2.3271	0.9616
Index-1.9B	1.91	48.02	0.0010	0.0009	1.9091	0.9995
SmolLM2-1.7B	1.71	49.95	0.0010	0.0008	1.7092	0.9995
StableLM2-1.6B	1.64	38.29	0.0010	0.0005	1.6395	0.9997
Fox-1-1.6B	1.61	42.25	0.0600	0.0322	1.6378	0.9807
GLM-Edge-1.5B	1.59	38.92	0.0060	0.0042	1.5858	0.9973
Qwen2.5-1.5B	1.54	59.84	0.0400	0.0308	1.5092	0.9800
Qwen2-1.5B	1.54	54.48	0.0500	0.0385	1.5015	0.9750
PLM-1.8B-Base	1.83	57.29	0.9090	0.4832	1.3968	0.7430

Table 14: The actual amount of parameters are calculated during the model inference.

8 Discussion: Future Works and Direction

Throughout the entire process of designing and training PLM, we draw lessons from investigating the needs of peripheral language models, empirically analyze the characteristics of LLMs on the edge, and explore the potential development of peripheral machine learning. Our findings highlight the crucial importance of treating the training of peripheral LLMs as a co-design field that integrates both modeling and system development.

8.1 Future Works

Based on the empirical cases in PLM design, training and deployment, we discuss the future works:

Peripheral LLM Adaptation To enable personalized language models on resource-constrained edge devices, we will develop efficient on-device adaptation techniques. This includes sparse update mechanisms for selective parameter modification [54], quantization-aware adaptation for low-precision fine-tuning [55], and memory-efficient gradient accumulation with incremental learning to distribute computational load across sessions.

Privacy-Preserving Federated Learning We will establish a federated learning framework for edge devices that ensures privacy through differential privacy, knowledge distillation, and secure aggregation [56]. Adaptive privacy budgeting will dynamically manage protection levels [57]. This enables bidirectional knowledge transfer, allowing cloud models to learn from privacy-sanitized edge updates and edge models to benefit from global improvements [56].

¹ The Activation Sparsity Rate calculation algorithm is illustrated in Appendix E

Edge-Cloud Collaborative Framework We will develop an edge-cloud framework that optimizes task distribution based on complexity and latency [58]. Edge models will handle simple, real-time queries, while complex tasks will be delegated to the cloud. Efficient communication channels will minimize data transfer and maintain contextual coherence. Dynamic task allocation [59] based on various factors will create an adaptive system, providing users with a seamless experience that combines immediate responses with deep reasoning capabilities.

Omni-MLLM and Enhanced Capabilities We will expand PLM to a multimodal model [60, 61], capable of processing and integrating diverse data types such as text, images, audio, and video to enable advanced applications like visual question answering, image captioning, and multimodal robotics. This enhancement will allow the model to perform tasks requiring cross-modal understanding, such as aligning video footage with textual instructions or analyzing 3D engineering data alongside textual descriptions. Model scaling will be achieved through expansion techniques [62]. Reasoning abilities will be improved by fine-tuning with distilled reasoning data, math and code capabilities will be enhanced with RL and rule-verifiable data [11]. Furthermore, the overall capabilities of PLM could be enhanced by integrating its domain-specialized counterpart [63] using tools like MergeKit [64]. Long-context modeling skills can be further improved through RAG-like methods [65]. Lastly, detecting and mitigating hallucinations [66] remains a crucial aspect of refinement.

Small Language Model for Reasoning We will investigate methodologies to enhance the reasoning capabilities of SLMs while preserving computational efficiency. Knowledge distillation [67] and supervised fine-tuning [11] are proven techniques to transfer knowledge from larger models, thus improving the accuracy of reasoning without significantly increasing resource demands. RL also presents a viable approach for optimizing reasoning processes; however, SLMs often face challenges with sparse reward signals when utilizing RL. Process-based reinforcement learning techniques [68, 35] may offer a more effective solution to guide SLMs. During the inference stage, adaptive test-time scaling emerges as a highly promising research direction, enabling dynamic adjustment of computational pathways based on input complexity to ensure efficient inference. Additionally, generative reward models [69] can provide supplementary supervision to SLMs, further boosting their reasoning performance. These advancements are poised to significantly elevate the reasoning capabilities of SLMs. Additionally, introducing peripheral language models in multi-agent scenarios can leverage Multi-Agent Reinforcement Learning (MARL) to elicit meta-thinking behaviors [70], enabling them to engage in reflective reasoning and navigate complex decision-making more effectively.

8.2 Direction

Empirically, MLA is designed to reduce the memory footprint of the Key-Value (KV) cache during inference by compressing key and value representations into a latent vector. This compression can alleviate memory bottlenecks, which is beneficial for deploying LLMs on edge devices with limited resources.

However, MLA introduces additional computational overhead due to the need to decompress the latent vectors during attention computations. This decompression step increases the number of matrix multiplications, potentially impacting inference speed [71]. For edge devices, which often have constraints on both memory and processing power, this trade-off between reduced memory usage and increased computational demand must be carefully considered.

Consequently, while MLA can help manage memory limitations on edge devices, its suitability depends on the specific balance between memory capacity and computational capabilities of the target hardware. Evaluating this trade-off is crucial to determine if MLA is appropriate for a given edge deployment scenario.

On the other hand, from the MLSys co-design perspective, the future of sparse LLMs hinges on a deep integration of algorithmic sparsity with hardware optimizations [72]. This involves designing custom accelerators that can efficiently handle sparse operations, optimizing memory architectures to minimize data movement, and implementing on-chip mechanisms for dynamic sparsity management. Hardware-aware sparsity [73] is crucial for realizing the potential efficiency gains of sparse LLMs, enabling faster inference and training while reducing energy consumption.

System-level optimizations are equally vital. This includes developing efficient sparse data formats, optimizing communication protocols for distributed training, and leveraging compiler optimizations to exploit sparsity in LLMs [74]. Memory hierarchy optimization and power efficiency are also critical considerations. By creating systems that are aware of sparsity patterns and can dynamically adjust resource allocation, we can unlock the full potential of sparse LLMs. This necessitates the creation of libraries and frameworks that can handle sparse data formats seamlessly across different hardware platforms.

Ultimately, the future direction emphasizes algorithm-hardware co-design [75]. This involves developing training algorithms that produce hardware-friendly sparsity patterns [76, 77], enabling dynamic sparsity adaptation during runtime [78, 79], and combining sparsity with quantization techniques to further reduce computational and memory

footprints [80]. By tightly coupling algorithmic innovations with hardware capabilities, we can create systems that can efficiently execute sparse LLMs, leading to significant advances in performance, energy efficiency, and scalability. This holistic approach will pave the way for the widespread deployment of sparse LLMs in resource-constrained environments.

The deployment of language models in peripheral scenario presents unique challenges and requirements distinct from cloud-based implementations. Our research identifies four critical directions that guide the development of effective edge-side models.

- Edge-side models require rapid response to meet time-sensitive application demands, as high latency significantly reduces their utility [81]. To achieve this within fixed hardware constraints, architectural innovations must prioritize inference speed without compromising model quality [82].
- Edge-side models enhance privacy by processing data locally, mitigating risks associated with remote server transmission [83]. To maintain this privacy, models must effectively extract information from limited local data while adhering to strict data movement restrictions.
- Edge models must be highly resource-efficient to avoid impacting primary device functions, operating within strict computational and storage limits. This requires model compression [84], efficient attention mechanisms [85], and dynamic resource allocation [86] to ensure they act as auxiliary, not primary, resource consumers.
- Power efficiency is paramount for edge models on battery-powered devices, as extended computation directly impacts battery life and user experience. Therefore, energy consumption must be a primary design consideration, employing techniques like sparse activation and precision reduction to minimize power draw without sacrificing performance [87].

Rapid response, privacy, resource efficiency, and power consumption are not mere limitations, but core challenges driving the development of peripheral LLMs. By focusing on these parameters, we aim to enable seamless integration of intelligent AI capabilities into peripheral and edge devices, delivering real-time responses while prioritizing user privacy and respecting device limitations.

9 Conclusion

We present PLM—an Edge Language Model optimized for resource-limited devices through a co-designed architecture combining Multi-head Latent Attention and squared ReLU for enhanced sparsity and reduced memory usage. PLM surpasses existing small language models on standard benchmarks and runs efficiently on devices ranging from PCs to mobile phones and Raspberry Pis. Moreover, we discuss the future direction of LLM on the edge. Finally, we release PLM-1.8B-Base and PLM-1.8B-Instruct to foster further research in peripheral computing. Along with the design and training of PLM, we analyze the needs, features, and potential development of peripheral language models, highlighting the crucial importance of viewing peripheral LLMs as a co-design field that integrates both hardware and algorithm development.

References

- [1] Christopher Savoie. How to mitigate the enterprise security risks of llms, 2023.
- [2] Ahmad Faiz, Sotaro Kaneda, Ruhan Wang, Rita Osi, Prateek Sharma, Fan Chen, and Lei Jiang. Llmcarbon: Modeling the end-to-end carbon footprint of large language models. *arXiv preprint arXiv:2309.14393*, 2023.
- [3] Hanchen Li, Yuhan Liu, Yihua Cheng, Siddhant Ray, Kuntai Du, and Junchen Jiang. Chatterbox: Robust transport for llm token streaming under unstable network. *arXiv preprint arXiv:2401.12961*, 2024.
- [4] Zhouhan Lin, Cheng Deng, Le Zhou, Tianhang Zhang, Yi Xu, Yutong Xu, Zhongmou He, Yuanyuan Shi, Beiya Dai, Yunchong Song, et al. Geogalactica: A scientific large language model in geoscience. *arXiv preprint* arXiv:2401.00434, 2023.
- [5] Zhenyan Lu, Xiang Li, Dongqi Cai, Rongjie Yi, Fangming Liu, Xiwen Zhang, Nicholas D Lane, and Mengwei Xu. Small language models: Survey, measurements, and insights. *arXiv preprint arXiv:2409.15790*, 2024.
- [6] An Yang, Baosong Yang, Binyuan Hui, Bo Zheng, Bowen Yu, Chang Zhou, Chengpeng Li, Chengyuan Li, Dayiheng Liu, Fei Huang, et al. Qwen2 technical report. *arXiv preprint arXiv:2407.10671*, 2024.
- [7] An Yang, Baosong Yang, Beichen Zhang, Binyuan Hui, Bo Zheng, Bowen Yu, Chengyuan Li, Dayiheng Liu, Fei Huang, Haoran Wei, et al. Qwen2.5 technical report. *arXiv preprint arXiv:2412.15115*, 2024.
- [8] Shengding Hu, Yuge Tu, Xu Han, Chaoqun He, Ganqu Cui, Xiang Long, Zhi Zheng, Yewei Fang, Yuxiang Huang, Weilin Zhao, et al. Minicpm: Unveiling the potential of small language models with scalable training strategies. *arXiv preprint arXiv:2404.06395*, 2024.
- [9] Loubna Ben Allal, Anton Lozhkov, Elie Bakouch, Gabriel Martín Blázquez, Lewis Tunstall, Agustín Piqueres, Andres Marafioti, Cyril Zakka, Leandro von Werra, and Thomas Wolf. Smollm2 with great data, comes great performance, 2024.
- [10] Yiwen Hu, Huatong Song, Jia Deng, Jiapeng Wang, Jie Chen, Kun Zhou, Yutao Zhu, Jinhao Jiang, Zican Dong, Wayne Xin Zhao, et al. Yulan-mini: An open data-efficient language model. *arXiv preprint arXiv:2412.17743*, 2024.
- [11] Daya Guo, Dejian Yang, Haowei Zhang, Junxiao Song, Ruoyu Zhang, Runxin Xu, Qihao Zhu, Shirong Ma, Peiyi Wang, Xiao Bi, et al. Deepseek-r1: Incentivizing reasoning capability in llms via reinforcement learning. *arXiv* preprint arXiv:2501.12948, 2025.
- [12] Ji Lin, Jiaming Tang, Haotian Tang, Shang Yang, Wei-Ming Chen, Wei-Chen Wang, Guangxuan Xiao, Xingyu Dang, Chuang Gan, and Song Han. Awq: Activation-aware weight quantization for on-device llm compression and acceleration. *Proceedings of Machine Learning and Systems*, 6:87–100, 2024.
- [13] Elias Frantar, Saleh Ashkboos, Torsten Hoefler, and Dan Alistarh. Gptq: Accurate post-training quantization for generative pre-trained transformers. *arXiv preprint arXiv:2210.17323*, 2022.
- [14] MLC team. MLC-LLM, 2023-2025.
- [15] Tianqi Chen, Thierry Moreau, Ziheng Jiang, Lianmin Zheng, Eddie Yan, Haichen Shen, Meghan Cowan, Leyuan Wang, Yuwei Hu, Luis Ceze, et al. {TVM}: An automated {End-to-End} optimizing compiler for deep learning. In 13th USENIX Symposium on Operating Systems Design and Implementation (OSDI 18), pages 578–594, 2018.
- [16] llama.cpp team. llama.cpp, 2023-2025.
- [17] Yixin Song, Zeyu Mi, Haotong Xie, and Haibo Chen. Powerinfer: Fast large language model serving with a consumer-grade gpu. In *Proceedings of the ACM SIGOPS 30th Symposium on Operating Systems Principles*, pages 590–606, 2024.
- [18] Zhenliang Xue, Yixin Song, Zeyu Mi, Le Chen, Yubin Xia, and Haibo Chen. Powerinfer-2: Fast large language model inference on a smartphone. *arXiv preprint arXiv:2406.06282*, 2024.
- [19] Woosuk Kwon, Zhuohan Li, Siyuan Zhuang, Ying Sheng, Lianmin Zheng, Cody Hao Yu, Joseph Gonzalez, Hao Zhang, and Ion Stoica. Efficient memory management for large language model serving with pagedattention. In *Proceedings of the 29th Symposium on Operating Systems Principles*, pages 611–626, 2023.
- [20] Lianmin Zheng, Liangsheng Yin, Zhiqiang Xie, Chuyue Sun, Jeff Huang, Cody Hao Yu, Shiyi Cao, Christos Kozyrakis, Ion Stoica, Joseph E Gonzalez, et al. Sglang: Efficient execution of structured language model programs. *arXiv preprint arXiv:2312.07104*, 2024.
- [21] Keivan Alizadeh, Iman Mirzadeh, Dmitry Belenko, Karen Khatamifard, Minsik Cho, Carlo C Del Mundo, Mohammad Rastegari, and Mehrdad Farajtabar. Llm in a flash: Efficient large language model inference with limited memory. *arXiv preprint arXiv:2312.11514*, 2023.

[22] Yixin Song, Haotong Xie, Zhengyan Zhang, Bo Wen, Li Ma, Zeyu Mi, and Haibo Chen. Turbo sparse: Achieving llm sota performance with minimal activated parameters. *arXiv preprint arXiv:2406.05955*, 2024.

- [23] Iman Mirzadeh, Keivan Alizadeh, Sachin Mehta, Carlo C Del Mundo, Oncel Tuzel, Golnoosh Samei, Mohammad Rastegari, and Mehrdad Farajtabar. Relu strikes back: Exploiting activation sparsity in large language models. *arXiv preprint arXiv:2310.04564*, 2023.
- [24] David So, Wojciech Mańke, Hanxiao Liu, Zihang Dai, Noam Shazeer, and Quoc V Le. Searching for efficient transformers for language modeling. *Advances in neural information processing systems*, 34:6010–6022, 2021.
- [25] Aixin Liu, Bei Feng, Bin Wang, Bingxuan Wang, Bo Liu, Chenggang Zhao, Chengqi Dengr, Chong Ruan, Damai Dai, Daya Guo, et al. Deepseek-v2: A strong, economical, and efficient mixture-of-experts language model. *arXiv* preprint arXiv:2405.04434, 2024.
- [26] Jianlin Su, Murtadha Ahmed, Yu Lu, Shengfeng Pan, Wen Bo, and Yunfeng Liu. Roformer: Enhanced transformer with rotary position embedding. *Neurocomputing*, 568:127063, 2024.
- [27] Jupinder Parmar, Shrimai Prabhumoye, Joseph Jennings, Mostofa Patwary, Sandeep Subramanian, Dan Su, Chen Zhu, Deepak Narayanan, Aastha Jhunjhunwala, Ayush Dattagupta, et al. Nemotron-4 15b technical report. arXiv preprint arXiv:2402.16819, 2024.
- [28] Zhengyan Zhang, Yixin Song, Guanghui Yu, Xu Han, Yankai Lin, Chaojun Xiao, Chenyang Song, Zhiyuan Liu, Zeyu Mi, and Maosong Sun. Relu2 wins: Discovering efficient activation functions for sparse llms. *arXiv preprint arXiv:2402.03804*, 2024.
- [29] Wayne Xin Zhao, Kun Zhou, Junyi Li, Tianyi Tang, Xiaolei Wang, Yupeng Hou, Yingqian Min, Beichen Zhang, Junjie Zhang, Zican Dong, et al. A survey of large language models. arXiv preprint arXiv:2303.18223, 2023.
- [30] Yang Liu, Jiahuan Cao, Chongyu Liu, Kai Ding, and Lianwen Jin. Datasets for large language models: A comprehensive survey. *arXiv preprint arXiv:2402.18041*, 2024.
- [31] David Wood, Boris Lublinsky, Alexy Roytman, Shivdeep Singh, Constantin Adam, Abdulhamid Adebayo, Sungeun An, Yuan Chi Chang, Xuan-Hong Dang, Nirmit Desai, et al. Data-prep-kit: getting your data ready for llm application development. *arXiv preprint arXiv:2409.18164*, 2024.
- [32] Ruibo Liu, Jerry Wei, Fangyu Liu, Chenglei Si, Yanzhe Zhang, Jinmeng Rao, Steven Zheng, Daiyi Peng, Diyi Yang, Denny Zhou, et al. Best practices and lessons learned on synthetic data for language models. *arXiv preprint arXiv:2404.07503*, 2024.
- [33] Loubna Ben Allal, Anton Lozhkov, Guilherme Penedo, Thomas Wolf, and Leandro von Werra. Cosmopedia, 2024.
- [34] Yiwei Qin, Xuefeng Li, Haoyang Zou, Yixiu Liu, Shijie Xia, Zhen Huang, Yixin Ye, Weizhe Yuan, Hector Liu, Yuanzhi Li, et al. O1 replication journey: A strategic progress report–part 1. *arXiv preprint arXiv:2410.18982*, 2024.
- [35] Jun Wang, Meng Fang, Ziyu Wan, Muning Wen, Jiachen Zhu, Anjie Liu, Ziqin Gong, Yan Song, Lei Chen, Lionel M Ni, et al. Openr: An open source framework for advanced reasoning with large language models. *arXiv* preprint arXiv:2410.09671, 2024.
- [36] Cheng Deng, Tianhang Zhang, Zhongmou He, Qiyuan Chen, Yuanyuan Shi, Yi Xu, Luoyi Fu, Weinan Zhang, Xinbing Wang, Chenghu Zhou, et al. K2: A foundation language model for geoscience knowledge understanding and utilization. In *Proceedings of the 17th ACM International Conference on Web Search and Data Mining*, pages 161–170, 2024.
- [37] Nathan Lambert, Jacob Morrison, Valentina Pyatkin, Shengyi Huang, Hamish Ivison, Faeze Brahman, Lester James V. Miranda, Alisa Liu, Nouha Dziri, Shane Lyu, Yuling Gu, Saumya Malik, Victoria Graf, Jena D. Hwang, Jiangjiang Yang andRonan Le Bras andOyvind Tafjord andChris Wilhelm andLuca Soldaini, Noah A. Smith, Yizhong Wang, Pradeep Dasigi, and Hannaneh Hajishirzi. Tülu 3: Pushing frontiers in open language model post-training. 2024.
- [38] Ganqu Cui, Lifan Yuan, Ning Ding, Guanming Yao, Wei Zhu, Yuan Ni, Guotong Xie, Zhiyuan Liu, and Maosong Sun. Ultrafeedback: Boosting language models with high-quality feedback, 2023.
- [39] Martin Weyssow, Aton Kamanda, Xin Zhou, and Houari Sahraoui. Codeultrafeedback: An Ilm-as-a-judge dataset for aligning large language models to coding preferences. *arXiv preprint arXiv:2403.09032*, 2024.
- [40] Zhengxiao Du, Aohan Zeng, Yuxiao Dong, and Jie Tang. Understanding emergent abilities of language models from the loss perspective. *arXiv* preprint arXiv:2403.15796, 2024.

[41] Xin Dong, Yonggan Fu, Shizhe Diao, Wonmin Byeon, Zijia Chen, Ameya Sunil Mahabaleshwarkar, Shih-Yang Liu, Matthijs Van Keirsbilck, Min-Hung Chen, Yoshi Suhara, et al. Hymba: A hybrid-head architecture for small language models. *arXiv preprint arXiv:2411.13676*, 2024.

- [42] Kaiming He, Xiangyu Zhang, Shaoqing Ren, and Jian Sun. Deep residual learning for image recognition. In *Proceedings of the IEEE conference on computer vision and pattern recognition*, pages 770–778, 2016.
- [43] Tianzhe Chu, Yuexiang Zhai, Jihan Yang, Shengbang Tong, Saining Xie, Dale Schuurmans, Quoc V Le, Sergey Levine, and Yi Ma. Sft memorizes, rl generalizes: A comparative study of foundation model post-training. *arXiv* preprint arXiv:2501.17161, 2025.
- [44] Yaowei Zheng, Richong Zhang, Junhao Zhang, Yanhan Ye, Zheyan Luo, Zhangchi Feng, and Yongqiang Ma. Llamafactory: Unified efficient fine-tuning of 100+ language models. In *Proceedings of the 62nd Annual Meeting of the Association for Computational Linguistics (Volume 3: System Demonstrations)*, Bangkok, Thailand, 2024. Association for Computational Linguistics.
- [45] Yongcheng Zeng, Xinyu Cui, Xuanfa Jin, Guoqing Liu, Zexu Sun, Quan He, Dong Li, Ning Yang, Jianye Hao, Haifeng Zhang, and Jun Wang. Aries: Stimulating self-refinement of large language models by iterative preference optimization, 2025.
- [46] Haoxiang Wang, Wei Xiong, Tengyang Xie, Han Zhao, and Tong Zhang. Interpretable preferences via multiobjective reward modeling and mixture-of-experts. In *EMNLP*, 2024.
- [47] Jiawei Liu, Chunqiu Steven Xia, Yuyao Wang, and Lingming Zhang. Is your code generated by chatGPT really correct? rigorous evaluation of large language models for code generation. In *Thirty-seventh Conference on Neural Information Processing Systems*, 2023.
- [48] Leo Gao, Jonathan Tow, Baber Abbasi, Stella Biderman, Sid Black, Anthony DiPofi, Charles Foster, Laurence Golding, Jeffrey Hsu, Alain Le Noac'h, Haonan Li, Kyle McDonell, Niklas Muennighoff, Chris Ociepa, Jason Phang, Laria Reynolds, Hailey Schoelkopf, Aviya Skowron, Lintang Sutawika, Eric Tang, Anish Thite, Ben Wang, Kevin Wang, and Andy Zou. A framework for few-shot language model evaluation, 07 2024.
- [49] Glm-edge, 2024.
- [50] Zijian Hu, Jipeng Zhang, Rui Pan, Zhaozhuo Xu, Salman Avestimehr, Chaoyang He, and Tong Zhang. Fox-1 technical report. *arXiv preprint arXiv:2411.05281*, 2024.
- [51] Index1.9b technical report, 2024.
- [52] Marco Bellagente, Jonathan Tow, Dakota Mahan, Duy Phung, Maksym Zhuravinskyi, Reshinth Adithyan, James Baicoianu, Ben Brooks, Nathan Cooper, Ashish Datta, et al. Stable lm 2 1.6 b technical report. *arXiv preprint arXiv:2402.17834*, 2024.
- [53] Saurav Muralidharan, Sharath Turuvekere Sreenivas, Raviraj Bhuminand Joshi, Marcin Chochowski, Mostofa Patwary, Mohammad Shoeybi, Bryan Catanzaro, Jan Kautz, and Pavlo Molchanov. Compact language models via pruning and knowledge distillation. In *The Thirty-eighth Annual Conference on Neural Information Processing Systems*, 2024.
- [54] Jesus Rios, Pierre Dognin, Ronny Luss, and Karthikeyan N Ramamurthy. Sparsity may be all you need: Sparse random parameter adaptation. *arXiv preprint arXiv:2502.15975*, 2025.
- [55] Se Jung Kwon, Jeonghoon Kim, Jeongin Bae, Kang Min Yoo, Jin-Hwa Kim, Baeseong Park, Byeongwook Kim, Jung-Woo Ha, Nako Sung, and Dongsoo Lee. Alphatuning: Quantization-aware parameter-efficient adaptation of large-scale pre-trained language models. *arXiv preprint arXiv:2210.03858*, 2022.
- [56] Marco Arazzi, Mert Cihangiroglu, Serena Nicolazzo, and Antonino Nocera. Secure federated data distillation. *arXiv preprint arXiv:2502.13728*, 2025.
- [57] Zhiqiang Wang, Xinyue Yu, Qianli Huang, and Yongguang Gong. An adaptive differential privacy method based on federated learning. *arXiv preprint arXiv:2408.08909*, 2024.
- [58] Hongpeng Jin and Yanzhao Wu. Ce-collm: Efficient and adaptive large language models through cloud-edge collaboration. *arXiv preprint arXiv:2411.02829*, 2024.
- [59] Yuqing Wang and Xiao Yang. Research on edge computing and cloud collaborative resource scheduling optimization based on deep reinforcement learning. *arXiv preprint arXiv:2502.18773*, 2025.
- [60] Chaoyou Fu, Haojia Lin, Zuwei Long, Yunhang Shen, Meng Zhao, Yifan Zhang, Shaoqi Dong, Xiong Wang, Di Yin, Long Ma, et al. Vita: Towards open-source interactive omni multimodal llm. *arXiv preprint* arXiv:2408.05211, 2024.

[61] Qingpei Guo, Kaiyou Song, Zipeng Feng, Ziping Ma, Qinglong Zhang, Sirui Gao, Xuzheng Yu, Yunxiao Sun, Jingdong Chen, Ming Yang, et al. M2-omni: Advancing omni-mllm for comprehensive modality support with competitive performance. *arXiv* preprint arXiv:2502.18778, 2025.

- [62] Yite Wang, Jiahao Su, Hanlin Lu, Cong Xie, Tianyi Liu, Jianbo Yuan, Haibin Lin, Ruoyu Sun, and Hongxia Yang. Lemon: Lossless model expansion. *arXiv preprint arXiv:2310.07999*, 2023.
- [63] TinyR1 Team. Superdistillation achieves near-r1 performance with just 5
- [64] Charles Goddard, Shamane Siriwardhana, Malikeh Ehghaghi, Luke Meyers, Vladimir Karpukhin, Brian Benedict, Mark McQuade, and Jacob Solawetz. Arcee's mergekit: A toolkit for merging large language models. In *Proceedings of the 2024 Conference on Empirical Methods in Natural Language Processing: Industry Track*, pages 477–485, 2024.
- [65] Qingfa Xiao, Jiachuan Wang, Haoyang Li, Cheng Deng, Jiaqi Tang, Shuangyin Li, Yongqi Zhang, Jun Wang, and Lei Chen. Activation-aware probe-query: Effective key-value retrieval for long-context llms inference. *arXiv* preprint arXiv:2502.13542, 2025.
- [66] Tianhang Zhang, Lin Qiu, Qipeng Guo, Cheng Deng, Yue Zhang, Zheng Zhang, Chenghu Zhou, Xinbing Wang, and Luoyi Fu. Enhancing uncertainty-based hallucination detection with stronger focus. *arXiv* preprint *arXiv*:2311.13230, 2023.
- [67] Gemma Team, Morgane Riviere, Shreya Pathak, Pier Giuseppe Sessa, Cassidy Hardin, Surya Bhupatiraju, Léonard Hussenot, Thomas Mesnard, Bobak Shahriari, Alexandre Ramé, et al. Gemma 2: Improving open language models at a practical size. *arXiv preprint arXiv:2408.00118*, 2024.
- [68] Zhenru Zhang, Chujie Zheng, Yangzhen Wu, Beichen Zhang, Runji Lin, Bowen Yu, Dayiheng Liu, Jingren Zhou, and Junyang Lin. The lessons of developing process reward models in mathematical reasoning. *arXiv* preprint *arXiv*:2501.07301, 2025.
- [69] Dakota Mahan, Duy Van Phung, Rafael Rafailov, Chase Blagden, Nathan Lile, Louis Castricato, Jan-Philipp Fränken, Chelsea Finn, and Alon Albalak. Generative reward models. *arXiv preprint arXiv:2410.12832*, 2024.
- [70] Ziyu Wan, Yunxiang Li, Yan Song, Hanjing Wang, Linyi Yang, Mark Schmidt, Jun Wang, Weinan Zhang, Shuyue Hu, and Ying Wen. Rema: Learning to meta-think for llms with multi-agent reinforcement learning. 2025.
- [71] Jiashi Li. Flashmla: Efficient mla decoding kernel. https://github.com/deepseek-ai/FlashMLA, 2025.
- [72] Jiajun Xu, Zhiyuan Li, Wei Chen, Qun Wang, Xin Gao, Qi Cai, and Ziyuan Ling. On-device language models: A comprehensive review. *arXiv preprint arXiv:2409.00088*, 2024.
- [73] Jingyang Yuan, Huazuo Gao, Damai Dai, Junyu Luo, Liang Zhao, Zhengyan Zhang, Zhenda Xie, YX Wei, Lean Wang, Zhiping Xiao, et al. Native sparse attention: Hardware-aligned and natively trainable sparse attention. *arXiv* preprint arXiv:2502.11089, 2025.
- [74] Ningxin Zheng, Huiqiang Jiang, Quanlu Zhang, Zhenhua Han, Lingxiao Ma, Yuqing Yang, Fan Yang, Chengruidong Zhang, Lili Qiu, Mao Yang, et al. Pit: Optimization of dynamic sparse deep learning models via permutation invariant transformation. In *Proceedings of the 29th Symposium on Operating Systems Principles*, pages 331–347, 2023.
- [75] Li Ding, Jun Liu, Shan Huang, and Guohao Dai. Vida: Video diffusion transformer acceleration with differential approximation and adaptive dataflow. In *Proceedings of the 30th Asia and South Pacific Design Automation Conference*, ASPDAC '25, page 148–154, New York, NY, USA, 2025. Association for Computing Machinery.
- [76] Abhinav Agarwalla, Abhay Gupta, Alexandre Marques, Shubhra Pandit, Michael Goin, Eldar Kurtic, Kevin Leong, Tuan Nguyen, Mahmoud Salem, Dan Alistarh, et al. Enabling high-sparsity foundational llama models with efficient pretraining and deployment. *arXiv preprint arXiv:2405.03594*, 2024.
- [77] Elias Frantar and Dan Alistarh. Sparsegpt: Massive language models can be accurately pruned in one-shot. In *International Conference on Machine Learning*, pages 10323–10337. PMLR, 2023.
- [78] Shang Yang, Junxian Guo, Haotian Tang, Qinghao Hu, Guangxuan Xiao, Jiaming Tang, Yujun Lin, Zhijian Liu, Yao Lu, and Song Han. Lserve: Efficient long-sequence llm serving with unified sparse attention. *arXiv* preprint *arXiv*:2502.14866, 2025.
- [79] Qihui Zhou, Peiqi Yin, Pengfei Zuo, and James Cheng. Progressive sparse attention: Algorithm and system co-design for efficient attention in llm serving, 2025.
- [80] Zhenyu Zhang, Shiwei Liu, Runjin Chen, Bhavya Kailkhura, Beidi Chen, and Atlas Wang. Q-hitter: A better token oracle for efficient llm inference via sparse-quantized kv cache. *Proceedings of Machine Learning and Systems*, 6:381–394, 2024.

[81] Mingjin Zhang, Xiaoming Shen, Jiannong Cao, Zeyang Cui, and Shan Jiang. Edgeshard: Efficient llm inference via collaborative edge computing. *IEEE Internet of Things Journal*, 2024.

- [82] Yue Zheng, Yuhao Chen, Bin Qian, Xiufang Shi, Yuanchao Shu, and Jiming Chen. A review on edge large language models: Design, execution, and applications. *ACM Computing Surveys*, 2024.
- [83] Zhongzhi Yu, Zheng Wang, Yuhan Li, Ruijie Gao, Xiaoya Zhou, Sreenidhi Reddy Bommu, Yang Zhao, and Yingyan Lin. Edge-Ilm: Enabling efficient large language model adaptation on edge devices via unified compression and adaptive layer voting. In *Proceedings of the 61st ACM/IEEE Design Automation Conference*, pages 1–6, 2024.
- [84] Fred Hohman, Mary Beth Kery, Donghao Ren, and Dominik Moritz. Model compression in practice: Lessons learned from practitioners creating on-device machine learning experiences. In *Proceedings of the 2024 CHI Conference on Human Factors in Computing Systems*, pages 1–18, 2024.
- [85] Feiyang Chen, Yu Cheng, Lei Wang, Yuqing Xia, Ziming Miao, Lingxiao Ma, Fan Yang, Jilong Xue, Zhi Yang, Mao Yang, et al. Attentionengine: A versatile framework for efficient attention mechanisms on diverse hardware platforms. *arXiv* preprint arXiv:2502.15349, 2025.
- [86] Lavanya Shanmugam, Suhas Jangoan, and Kapil Kumar Sharma. Dynamic resource allocation in edge computing for ai/ml applications: Architectural framework and optimization techniques. *Journal of Knowledge Learning and Science Technology ISSN:* 2959-6386 (online), 2(2):385–397, 2023.
- [87] Varatheepan Paramanayakam, Andreas Karatzas, Iraklis Anagnostopoulos, and Dimitrios Stamoulis. Less is more: Optimizing function calling for llm execution on edge devices. *arXiv preprint arXiv:2411.15399*, 2024.
- [88] Rafael Rafailov, Archit Sharma, Eric Mitchell, Christopher D Manning, Stefano Ermon, and Chelsea Finn. Direct preference optimization: Your language model is secretly a reward model. *Advances in Neural Information Processing Systems*, 36:53728–53741, 2023.

A Architecture Searching Experiments

We detail our sandbox experiments of model architecture. Through these experiments, we seek to find the most appropriate configuration making a balance between performance and computation. Therefore, the hyperparameters n_{layer} , d_{head} , and n_{head} should be focused. We have conducted several architecture experiments and present the most relevant candidates here. We present the candidate configuration in table 15, and computation details in table 16.

Table 15: Architectures search candidates.

No.	#Params	n _{layer}	d_{model}	n_{head}	d_{head}	d_{ffn}	kv_{rank}	q_{rank}	d_{rope}
1	1.54B	28	2816	44	64	7040	256	768	32
2	1.21B	32	2304	36	64	5760	256	768	32
3	1.47B	32	2560	40	64	6400	256	768	32
4	1.36B	36	2304	36	64	5760	256	768	32
5	1.51B	40	2304	36	64	5760	256	768	32
6	1.55B	36	2048	32	64	8192	256	768	32
7	1.54B	32	2048	16	128	8192	512	1536	64

Table 16: Hardware-aware attributes of the candidates, tested on Raspberry Pi.

	MACs	FLOPs	FWD+BWD	FWD+BWD	Fac	etors	TTFT	Time/Layer	Token Rate	Peak Memory
No.	(G)	(G)	(GMACs)	(GFLOPs)	MACs/Param	FLOPs/Param	(ms)	(ms)	(tok/s)	(GB)
1	206	412	618	1240	103	205	9075	324	7.8E-2	7.0E-5
2	164	327	491	982	102	205	3178	99	2.6E-1	7.8E-5
3	198	396	594	1190	104	208	3775	118	2.2E-1	6.6E-5
4	184	368	552	1100	105	209	3592	100	2.3E-1	6.8E-5
5	205	409	614	1230	107	214	4040	101	2.1E-1	7.1E-5
6	207	414	622	1240	109	218	3995	111	2.2E-1	7.2E-5
7	203	406	609	1220	108	216	3354	105	2.6E-1	6.7E-5

Table 17: Sandbox experiments hyperparameters.

Hyperparameter	Value
Global Batch Size	960
Micro Batch Size	3
Max Learning Rate	5.00E-04
Min Learning Rate	5.00E-06
Weight Decay	0.1
Adam β_1	0.9
Adam β_2	0.95
Clip Grad	1.0
Attention Dropout	0
Hidden Dropout	0
Sequence Length	4096

Table 18: Training data distribution and allocation.

Selected Size (B)	Training Allocation (B)	Normalized Ratio	Category
1485	59	0.59	English
518	22	0.22	Chinese
120	7	0.07	Chinese
50	2	0.02	Math
9	1	0.01	Math
226	10	0.10	Code
	1485 518 120 50 9	1485 59 518 22 120 7 50 2 9 1	1485 59 0.59 518 22 0.22 120 7 0.07 50 2 0.02 9 1 0.01

In each experiment, we strive to adopt our final pre-training configuration, as shown in the table Table 17, using WSD learning rate scheduler and a corpus with similar data distribution as the final pre-train corpus, shown in Table 18.

B Datasets

B.1 Pre-Train Dataset

Table 19: Training data distribution and allocation.

Phase	Data Source	Selected Size (B)	Training Allocation (B)	Normalized Ratio	Category
1	mlfoundations/dclm-baseline-1.0	1485	966	0.59	English
1	m-a-p/MAP-CC	518	363	0.22	Chinese
1	BAAI/CCI3-HQ	120	120	0.07	Chinese
1	EleutherAI/proof-pile-2	50	39	0.02	Math
1	GAIR/MathPile	9	9	0.01	Math
1	bigcode/starcoderdata	226	158	0.10	Code
2	HuggingFaceTB/smollm-corpus	222	220	0.4	English
2	allenai/dolmino-mix-1124/data/flan	74	80	0.15	English
2	opencsg/chinese-fineweb-edu-v2	221	120	0.22	Chinese
2	allenai/dolmino-mix-1124/data/pes2o	60	60	0.1	Paper
2	OpenCoder-LLM/opc-annealing-corpus	64	62	0.11	Code
2	bigcode/the-stack-v2	8	8	0.01	Code
3	HuggingFaceTB/smollm-corpus	220	100	0.36	English
3	opencsg/chinese-fineweb-edu-v2	221	40	0.14	Chinese
3	yulan-team/YuLan-Mini-Datasets	96	90	0.32	Code,QA
3	allenai/dolmino-mix-1124/data/math	11	10	0.04	Math
3	plm/sft-data	46	40	0.14	QA,MATH,Code

B.2 Internal Pre-Train Dataset

We utilized public available supervised fine-tuning datasets to re-structure into pre-train data. The collected datasets are listed in Table 22.

B.3 Post-Train Data

Supervised fine-tuning data Based on the collected SFT-like data, we gather and form the two phases SFT datasets, shown as Table 20.

Table 20: Datasets used in phase 1 and phase 2 of SFT.

Phase 1 Datasets	Phase 2 Datasets
allenai/tulu-3-sft-mixture	ibm/ProvoQ
teknium/GPTeacher-General-Instruct	ibm/AttaQ
01-OPEN/Open01-SFT	allenai/wildguardmix
01-OPEN/Open01-SFT-Ultra	allenai/tulu-3-sft-mixture
01-OPEN/Open01-SFT-Pro	hkust-nlp/dart-math-hard
causal-lm/ultrachat	hkust-nlp/dart-math-uniform
Open-Orca/SlimOrca	meta-math/MetaMathQA_GSM8K_zh
GAIR/lima	meta-math/MetaMathQA
BelleGroup/train_2M_CN	<pre>HuggingFaceTB/math_tasks</pre>
suolyer/webqa	allenai/tulu-3-sft-personas-math
YeungNLP/firefly-train-1.1M	nvidia/OpenMathInstruct-2
deepctrl/deepctrl-sft-data	BAAI/Infinity-Instruct
shibing624/sharegpt_gpt4	BAAI/IndustryInstruction
G. G.	BAAI/InfinityMATH
	BAAI/AquilaEdu-Instruct
	BAAI/AquilaMed-Instruct
	amztheory/codegen-instruct-python-1k
	amztheory/codegen-instruct-CPlus-1k
	AI-MO/NuminaMath-CoT
	nvidia/AceMath-Instruct-Training-Data
	glaiveai/glaive-code-assistant-v2
	sahil2801/CodeAlpaca-20k
	iamtarun/python_code_instructions_18k_alpac
	likaixin/InstructCoder
	Codegen/codegen-instruct
	hfl/ruozhiba_gpt4_turbo
	wiki_qa
	ultrachat_200k

Reinforcement learning with human feedback data. For the reinforcement learning with human feedback, we adopt the data from Table 21.

Table 21: Reinforcement learning with human feedback dataset.

No	Dataset	Sample	Class
1	allenai/llama-3.1-tulu-3-70b-preference-mixture	334302	General Dialogue
2	HuggingFaceH4/ultrafeedback_binarized	5120	General Dialogue
3	coseal/CodeUltraFeedback	9433	Code

Table 22: Supervised fine-tuning dataset collection.

No	Dataset	Sample	Class
1	ELM-Internal-Instruct	123569	Knowledge
2	amztheory/codegen-instruct-python-1k	1234	Code
3	amztheory/codegen-instruct-CPlus-1k	813	Code
4	PowerInfer/LONGCOT-Refine-500K	521921	Thought
5	PowerInfer/QWQ-LONGCOT-500K	498082	Thought
6	causal-lm/ultrachat	5084540	General
7	allenai/wildjailbreak	261538	Safety
8	ibm/ProvoQ	2705	Safety
9	ibm/AttaQ	1402	Safety
10	allenai/wildguardmix	37976	Safety
11	allenai/tulu-3-sft-mixture	939343	General
12	nvidia/ChatQA-Training-Data	442261	General
13	HuggingFaceTB/smoltalk	1098865	General
14	HuggingFaceH4/ultrachat_200k	515311	General Dialogue
15	WizardLMTeam/WizardLM evol instruct V2 196k	143000	General
16	anon8231489123/ShareGPT_Vicuna_unfiltered	94145	General
17	kanhatakeyama/wizardlm8x22b-logical-math-coding-sft	284303	logit
18	kanhatakeyama/logical-wizardlm-7b	21529967	logit
19	Open-Orca/SlimOrca-Dedup	363491	General
20	openchat/openchat_sharegpt4_dataset	105003	General
21	LDJnr/Capybara	16006	General Dialogue
22	hkust-nlp/deita-10k-v0	10000	General
23	hkust-nlp/vrt-baseline	590601	Math
24	hkust-nlp/dart-math-hard	585392	Math
25	hkust-nlp/dart-math-uniform	590705	Math
26	hkust-nlp/dart-math-pool-gsm8k	2738984	Math
27	hkust-nlp/dart-math-pool-math	1615233	Math
28	meta-math/MetaMathQA GSM8K zh	463370	Math
29	hkust-nlp/gsm8k-fix	7473	Math
30	meta-math/MetaMathQA-40K	40000	Math
31	meta-math/GSM8K zh	17582	Math
32	meta-math/GSM8K_Backward	2540	Math
33	meta-math/MetaMathQA	395000	Math
34	HuggingFaceTB/math tasks	21292	Math
35	pvduy/synth_code_preference_4k	4052	Code
36	allenai/RLVR-GSM	7473	Math
37	allenai/tulu-3-sft-personas-math	149960	Math
38	RUC-AIBOX/long_form_thought_data_5k	4922	Thought
39	nvidia/ChatQA2-Long-SFT-data	128000	General
40	nvidia/OpenMathInstruct-2	21972789	Math
41	mengfn/MathOdyssey	389	Math
42	mengfn/longthoughts-synth	14973	Thought
43	mengfn/MATH-clean	7500	Math
44	O1-OPEN/OpenO1-SFT	77685	Thought
45	BAAI/Infinity-Instruct	1456927	General
46	BAAI/IndustryInstruction	2706143	General
47	BAAI/InfinityMATH	101380	MATH
48	BAAI/IninityMATT BAAI/AquilaEdu-Instruct	269917	General
49	BAAI/AquilaMed-Instruct	318357	General
50	BAAI/Aquilalvied-Instruct BAAI/COIG	275985	Code
51	Codegen (LINK)	4535	Code
52		20022	Code
53	sahil2801/CodeAlpaca-20k		Code
53 54	iamtarun/python_code_instructions_18k_alpaca	18612	
	likaixin/InstructCoder	108391	Code
56	O1-OPEN/OpenO1-SFT-Pro	125894	Thought
	Total	60533509	

C Training Details

Table 23 presents the training hyperparameters used during the three phases of PLM pre-training, highlighting variations in the learning rate schedule, weight decay, batch sizes, and optimization parameters to facilitate effective model convergence across different training stages.

C.1 Pre-training

	_		
	PLM Per-train Phase 1	PLM Per-train Phase 2	PLM Per-train Phase 3
Global Batch Size	3744	3744	3744
Micro Batch Size	3	3	3
Learning Rate	3.00E-04	3.00E-04	3.00E-05
Min Learning Rate	3.00E-04	5.00E-06	0.00E+00
Lr Scheduler Type	Warm-up and Stable	Decay	Constant
Weight Decay	0.1	0.1	0.1
Adam Beta1	0.9	0.9	0.9
Adam Beta2	0.95	0.95	0.95
Clip Grad	1.0	1.0	1.0
Init Method Std	0.008	Null	Null
Attention Dropout	0	0	0
Hidden Dropout	0	0	0
Seq Length	4096	4096	4096
Epoch	1	1	1

Table 23: Training arguments for pre-training.

Figure 12 illustrates the validation loss curves across different training phases, demonstrating how the loss evolves as a function of the number of training tokens, with distinct trends for each phase reflecting the impact of different pre-training strategies on model performance.

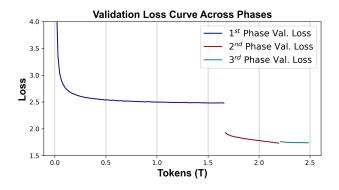


Figure 12: Validation loss curve across phases during training.

C.2 Supervised Fine-tuning

Table 24 details the training configurations used for the two phases of supervised fine-tuning in the PLM model, specifying batch sizes, learning rate schedules, and regularization techniques applied to refine the pre-trained model for downstream tasks.

Table 24: Training arguments for supervised fine-tuning.

	PLM SFT Phase 1	PLM SFT Phase 2
Global Batch Size	256	256
Micro Batch Size	4	4
Learning Rate	2.00E-05	2.00E-05
Min Learning Rate	0.00E+00	0.00E+00
Lr Scheduler Type	Cosine	Cosine
Weight Decay	0.1	0.1
Adam Beta1	0.9	0.9
Adam Beta2	0.95	0.95
Clip Grad	1	1
Attention Dropout	0	0
Hidden Dropout	0	0
Seq Length	4096	4096
Epoch	5	3

Figure 13 presents the supervised fine-tuning (SFT) loss curves across different training phases, showing the progressive reduction in loss as the model undergoes further refinement with fine-tuning, with noticeable differences in convergence between phases.

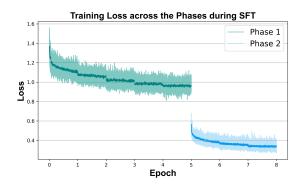


Figure 13: SFT loss curve across phases during training.

C.3 Preference Training

Table 25 outlines the training hyperparameters used during the two phases of Reinforcement Learning with Human Feedback (RLHF) for the PLM model, including batch sizes, learning rates, weight decay, Adam optimizer parameters, and specific RLHF-related coefficients such as α , β_{DPO} , and $\beta_{entropy}$, which influence the policy updates and reward shaping.

Table 25: Training Arguments for RLHF.

	PLM RLHF Phase 1	PLM RLHF Phase 2
Global Batch Size	128	128
Micro Batch Size	4	4
Leranging Rate	5.00E-07	1.00E-07
Min Learning Rate	5.00E-08	1.00E-08
Lr Scheduler Type	Cosine	Cosine
Weight Decay	0.1	0.1
Adam Beta1	0.9	0.9
Adam Beta2	0.95	0.95
Clip Grad	1	1
Attention Dropout	0	0
Hidden Dropout	0	0
Seq Length	1024	1024
Époch	1	1
$\dot{\alpha}$	0.8	0.8
β_{DPO}	0.1	0.1
β_{refine}	0.01	0.01
Temperature	-	0.7

Similar to DPO [88], we define the implicit reward as $\hat{r}(x,y) = \beta \log \frac{\pi_{\theta}(y|x)}{\pi_{\text{ref}}(y|x)}$, and the implicit reward accuracy is defined as the probability that $\beta \log \frac{\pi_{\theta}(y_w|x)}{\pi_{\text{ref}}(y_w|x)} > \beta \log \frac{\pi_{\theta}(y_t|x)}{\pi_{\text{ref}}(y_t|x)}$ holds for the preferred response y_w over the dispreferred response y_l . Figure 14 presents the implicit reward accuracy curves for the two phases of RLHF training, showing how the model's reward signal evolves over training steps, with phase 1 exhibiting higher fluctuations and phase 2 demonstrating a smoother upward trend, indicating progressive refinement in aligning model outputs with human preferences.

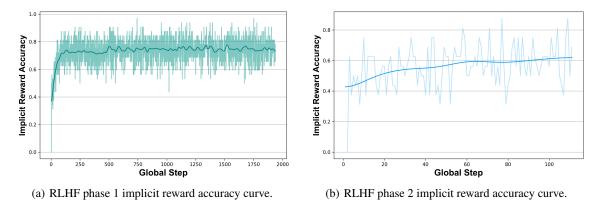


Figure 14: RLHF implicit reward accuracy curve for PLM.

Table 25 displays the Reinforcement Learning with Human Feedback (RLHF) training curves for PLM across two phases, illustrating the fluctuations in loss during phase 1 and the gradual stabilization observed in phase 2, reflecting the model's adaptation to preference-based learning.

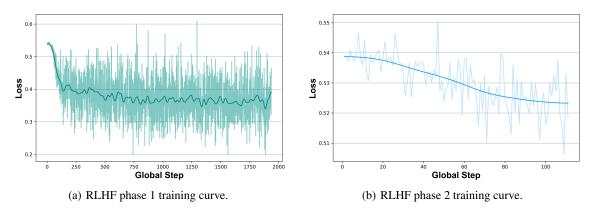


Figure 15: RLHF training curve for PLM.

D Computational Analysis

The primary mechanism of MLA involves transforming the Key-Value (KV) matrix into a low-rank representation. This is accomplished by decomposing the original KV matrix into the product of two smaller matrices, effectively creating latent vectors. During inference, only these latent vectors are cached, significantly reducing KV cache requirements compared to storing the full KV matrix. This approach mitigates the information loss associated with grouped-query attention (GQA) and multi-query attention (MQA), potentially enhancing model performance. While MLA reduces KV cache memory, it introduces additional computational overhead, similar to other low-rank adaptation methods like LoRA. This appendix analyzes the computational costs of MLA and GQA.

D.1 MLA

D.1.1 Definition

Let $h_t \in \mathbb{R}^d$ represent the input hidden state for the t-th token in the attention mechanism. The low-rank key-value joint compression state is denoted as $c_t^{KV} \in \mathbb{R}^{d_c}$, while the decompressed key and value for the i-th head are denoted by $k_{t,i}^C \in \mathbb{R}^{d_{\text{nope}}}$ and $v_{t,i}^C \in \mathbb{R}^{d_{\text{nope}}}$, respectively. The position-independent query for the i-th head is represented as $q_{t,i}^C \in \mathbb{R}^{d_{\text{nope}}}$. The computations for the attention mechanism proceed as follows:

$$\boldsymbol{c}_{t}^{KV} = W_{\text{DKV}}\boldsymbol{h}_{t}, \tag{8}$$

$$\boldsymbol{k}_{t,i}^{C} = W_{\mathrm{UK},i} \boldsymbol{c}_{t}^{KV}, \tag{9}$$

$$\boldsymbol{k}_{t}^{R} = \text{RoPE}\left(W_{KR}\boldsymbol{h}_{t}\right),\tag{10}$$

$$\mathbf{k}_{t,i} = \left[\mathbf{k}_{t}^{C}; \mathbf{k}_{t}^{R} \right], \tag{11}$$

$$\boldsymbol{q}_{t,i}^C = W_{\mathbf{Q},i}\boldsymbol{h}_t,\tag{12}$$

$$\boldsymbol{q}_{t,i}^{R} = \text{RoPE}\left(W_{\text{QR},i}\boldsymbol{h}_{t}\right),\tag{13}$$

$$\boldsymbol{q}_{t,i} = \left[\boldsymbol{q}_{t,i}^{C}; \boldsymbol{q}_{t,i}^{R} \right], \tag{14}$$

$$\boldsymbol{v}_{t,i}^{C} = W_{\text{UV},i} \boldsymbol{c}_{t}^{KV}, \tag{15}$$

where $W_{\mathrm{DKV}} \in \mathbb{R}^{d_{\mathrm{nope}} \times d_c}$ is the down-projection matrix for key-value compression, $W_{\mathrm{UK},i} \in \mathbb{R}^{d_{\mathrm{nope}} \times d_c}$ and $W_{\mathrm{UV},i} \in \mathbb{R}^{d_{\mathrm{nope}} \times d_c}$ are the up-projection matrices for decompressed key and value for the i-th head, $W_{\mathrm{KR}} \in \mathbb{R}^{d_{\mathrm{nope}} \times d}$ generates the shared positional key component via RoPE [26], and $W_{\mathrm{Q},i} \in \mathbb{R}^{d_{\mathrm{nope}} \times d}$ and $W_{\mathrm{QR}} \in \mathbb{R}^{d_{\mathrm{rope}} \times d}$ generate the position-independent and RoPE-enhanced query components for the i-th head.

The attention outputs $\{o_{t,i}\}$ are calculated as follows:

$$o_{t,i} = \sum_{j=1}^{t} \text{Softmax}_{j} \left(\frac{\boldsymbol{q}_{t,i}^{\top} \boldsymbol{k}_{j,i}}{\sqrt{d_{h}}} \right) \boldsymbol{v}_{j,i}^{C}, \tag{16}$$

where $d_h = d_{\text{nope}} + d_{\text{rope}}$ represents the total head dimension. The final output is obtained by combining the attention results from all heads through a linear projection:

$$u_t = W_0[o_{t,1}; o_{t,2}; \dots; o_{t,n_b}],$$
 (17)

where $W_0 \in \mathbb{R}^{d \times d_{\text{nope}} n_h}$ is the output projection matrix and n_h is the number of attention heads.

D.1.2 Prefill

Let the input sequence length be N. The computational complexity for projecting the context vector \boldsymbol{c}_t^{KV} is $\mathcal{O}(dd_cN)$. Subsequent projections for content-based keys $\boldsymbol{k}_{t,i}^C$ and values $\boldsymbol{v}_{t,i}^C$ require $\mathcal{O}(2d_cd_{\text{nope}}N)$ operations, while the query projection $\boldsymbol{q}_{t,i}^C$ incurs $\mathcal{O}(dd_{\text{nope}}N)$. For rotary position embeddings (RoPE), the projections for \boldsymbol{k}_t^R and $\boldsymbol{q}_{t,i}^R$ each demand $\mathcal{O}(dd_{\text{rope}}N)$, with an additional $\mathcal{O}(2(n_h+1)d_{\text{rope}}N)$ for applying RoPE transformations.

The total computational cost for generating keys $\{k_{t,i}\}$, queries $\{q_{t,i}\}$, and values $\{v_{t,i}\}$ combines these components:

$$\mathcal{O}\left(\left[2(n_h+1)d_{\text{rope}}+d_cd+d_{\text{rope}}d+n_h(d_{\text{nope}}+d_{\text{rope}})d+2n_hd_cd_{\text{nope}}\right]N\right).$$

Attention calculation involves pairwise interactions, contributing $\mathcal{O}\left(n_h(d_{\text{rope}}+2d_{\text{nope}})N^2\right)$ due to the quadratic dependence on sequence length. The output projection further adds $\mathcal{O}(d^2N)$.

Aggregating all terms, the overall computational complexity becomes:

 $Prefill_{mla} =$

$$\mathcal{O}\left(\left[2(n_{h}+1)d_{\text{rope}} + d_{c}d + d_{\text{rope}}d + n_{h}(d_{\text{nope}} + d_{\text{rope}})d + 2n_{h}d_{c}d_{\text{nope}} + d^{2}\right]N + n_{h}(d_{\text{rope}} + 2d_{\text{nope}})N^{2}\right). \tag{18}$$

This formulation highlights the linear and quadratic scaling components, emphasizing the interplay between sequence length N, head dimensions d_{rope} , d_{nope} , and model hyperparameters.

D.1.3 Decode

Consider an input sequence of length N-1. The computational complexity to generate the N-th token's joint compression state \boldsymbol{c}_N^{KV} is $\mathcal{O}(dd_c)$. Subsequent projections for the rotary position embedding (RoPE)-based key \boldsymbol{k}_N^R and query $\boldsymbol{q}_{N,i}^R$ each require $\mathcal{O}(dd_{\text{rope}})$, while the content-based query $\boldsymbol{q}_{N,i}^C$ incurs $\mathcal{O}(dd_{\text{nope}})$. The RoPE transformation further demands $\mathcal{O}(2(n_h+1)d_{\text{rope}})$. For historical tokens $t=1,\ldots,N$, the projections of content-based keys $\{\boldsymbol{k}_{t,i}^C\}$ and values $\{\boldsymbol{v}_{t,i}^C\}$ scale as $\mathcal{O}(2d_cd_{\text{nope}}N)$.

Attention computation involves aggregating interactions across the sequence, contributing $\mathcal{O}(n_h(d_{\text{rope}} + 2d_{\text{nope}})N)$, while the output projection requires $\mathcal{O}(d^2)$. Combining these components, the total computational cost is:

$$Generate_{mla} = \mathcal{O}\Big(2(n_h+1)d_{rope} + d_cd + d_{rope}d + n_h(d_{nope} + d_{rope})d + d^2 + n_h(d_{rope} + 2d_{nope} + 2d_cd_{nope})N\Big).$$

Caching mechanisms store the joint compression states $\{c_t^{KV}\}_{t=1,...,N-1}$ and RoPE keys $\{k_t^R\}_{t=1,...,N-1}$, with memory footprint:

Cache_{mla} =
$$(d_{\text{rope}} + d_c) \times \left(\frac{\text{bit width}}{8}\right) \times (N-1)$$
.

The latency of the decoder is governed by computational throughput and I/O bandwidth:

$$\begin{split} MLA\text{-}IO_{time} &= IO_{speed} \times Cache_{mla}, \\ MLA\text{-}Gengeate_{time} &= Compute_{speed} \times Generate_{mla}, \end{split}$$

where IO_{speed} and Compute_{speed} denote hardware-specific I/O and computational throughput rates. This formulation underscores the interplay between sequence length N, model dimensions, and hardware constraints in latency-critical decoding steps.

D.2 GQA

D.2.1 Definition

Let $h_t \in \mathbb{R}^d$ represent the input hidden state for the t-th token in the attention mechanism. The grouped key and value for the j-th kv head are denoted by $k_{t,j} \in \mathbb{R}^{d_{\rm h}}$ and $v_{t,j} \in \mathbb{R}^{d_{\rm h}}$, respectively. The position-independent query for the i-th head is represented as $q_{t,i} \in \mathbb{R}^{d_{\rm h}}$. The computations for the attention mechanism proceed as follows:

$$\boldsymbol{k}_{t,j} = \text{RoPE}\left(W_{\mathbf{K},j}\boldsymbol{h}_t\right),\tag{19}$$

$$q_{t,i} = \text{RoPE}\left(W_{0,i}h_t\right),\tag{20}$$

$$\boldsymbol{v}_{t,j}^C = W_{V,j} \boldsymbol{h}_t, \tag{21}$$

where $W_{K,j} \in \mathbb{R}^{d_h \times d}$ and $W_{V,j} \in \mathbb{R}^{d_h \times d}$ are the up-projection matrices for grouped key and value for the j-th kv head, and $W_{Q,i} \in \mathbb{R}^{d_h \times d}$ for the i-th head, respectively.

The attention outputs $\{o_{t,i}\}$ are calculated as follows:

$$o_{t,i} = \sum_{k=1}^{t} \operatorname{Softmax}_{k} \left(\frac{q_{t,i}^{\top} k_{k,i \text{ mod } n_{\text{kv_heads}}}}{\sqrt{d_{\text{h}}}} \right) v_{k,i \text{ mod } n_{\text{kv_heads}}},$$
(22)

where $d_h = d_{\text{nope}} + d_{\text{rope}}$ represents the total head dimension, $n_{\text{kv_heads}}$ is the number of kv heads. The final output is obtained by combining the attention results from all heads through a linear projection:

$$\boldsymbol{u}_t = W_0 \left[\boldsymbol{o}_{t,1}; \boldsymbol{o}_{t,2}; \dots; \boldsymbol{o}_{t,n_b} \right], \tag{23}$$

where $W_0 \in \mathbb{R}^{d \times d_{\text{nope}} n_h}$ is the output projection matrix and n_h is the number of attention heads.

D.2.2 Prefill

For an input sequence of length N, the computational complexity begins with the projection operations for keys $k_{t,j}$ and values $v_{t,j}$, each requiring $\mathcal{O}(2dd_hN)$ operations. The query projection $q_{t,i}$ further contributes $\mathcal{O}(dd_hN)$. Rotary Position Embedding (RoPE) transformations introduce an additional $\mathcal{O}(2(n_h + n_{\text{kv_heads}})d_hN)$, where n_h and $n_{\text{kv_heads}}$ denote the number of attention heads and key-value heads, respectively. Aggregating these components, the total cost to compute keys $\{k_{t,i}\}$, queries $\{q_{t,i}\}$, and values $\{v_{t,i}\}$ becomes:

$$\mathcal{O}\Big(\left[2(n_h + n_{\text{kv_heads}})d_{\text{h}} + d^2 + 2n_{\text{kv_heads}}d_{\text{h}}d\right]N\Big).$$

The attention mechanism scales quadratically with sequence length, demanding $\mathcal{O}(2n_hd_hN^2)$ operations due to pairwise token interactions. Following this, the output projection incurs $\mathcal{O}(d^2N)$.

Combining all terms, the total computational complexity for the prefill phase is:

$$Prefill_{gqa} = \mathcal{O}\left(\left[2(n_h + n_{\text{kv_heads}})d_h + 2d^2 + 2n_{\text{kv_heads}}d_hd\right]N + 2n_hd_hN^2\right).$$

This formulation highlights the dominant $\mathcal{O}(N^2)$ term from attention, alongside linear contributions from projections and RoPE. The interplay between model dimensions (d, d_h) , head counts $(n_h, n_{\text{kv_heads}})$, and sequence length N underscores the scalability challenges in large-context processing.

D.2.3 Decode

For an input sequence of length N-1, the decoder phase computes the N-th token's representations through successive transformations. Key and value projections $\boldsymbol{k}_{N,j}$ and $\boldsymbol{v}_{N,j}$ require $\mathcal{O}(2d_{\mathrm{h}}d)$ operations, while the query projection $\boldsymbol{q}_{N,i}$ incurs $\mathcal{O}(dd_{\mathrm{h}})$. Rotary Position Embedding (RoPE) adds $\mathcal{O}\big(2(n_h+n_{\mathrm{kv_heads}})d_{\mathrm{h}}\big)$, where n_h and $n_{\mathrm{kv_heads}}$ denote attention and key-value head counts.

The attention mechanism, operating over cached historical states, scales as $\mathcal{O}(2n_hd_hN)$, reflecting linear dependence on sequence length N. A final output projection contributes $\mathcal{O}(d^2)$. Aggregating all components, the total computational cost is:

Generate_{gqa} =
$$\mathcal{O}\left(2(n_h + n_{\text{kv_heads}})d_h + 2d^2 + 2n_{\text{kv_heads}}d_hd + 2n_hd_hN\right)$$
.

Caching historical keys $\{k_{t,j}\}$ and values $\{v_{t,j}\}$ for $t=1,\ldots,N-1$ demands memory:

$$\label{eq:cache} \text{Cache}_{\text{gqa}} = 2 \times n_{\text{kv_heads}} \times d_{\text{h}} \times \left(\frac{\text{bit width}}{8}\right) \times (N-1),$$

where bit width governs precision. Latency is determined by hardware throughput:

$$\begin{aligned} & GQA\text{-}IO_{time} = IO_{speed} \times Cache_{gqa}, \\ & GQA\text{-}Generate_{time} = Compute_{speed} \times Generate_{gqa}, \end{aligned}$$

with IO_{speed} and $Compute_{speed}$ representing I/O and computational bandwidth. This framework underscores the decoder's reliance on sequence length N, model dimensions (d, d_h) , and hardware constraints, emphasizing trade-offs between memory footprint and parallelizable computation.

E Activation Sparsity Determination Experiments

Algorithm 1 determine Activation Sparsity Rate This algorithm outlines a method for determining the optimal activation sparsity rate in an MLP layer, leveraging a gating mechanism (if available) and a benchmark dataset to maintain a target perplexity reduction of $\Delta ppl = 1$. The process involves computing the baseline activation, iterating through candidate sparsity rates, identifying threshold values to mask activations, and evaluating the modified model's perplexity to determine if the sparsity condition is met. If a valid sparsity rate is found that satisfies the target perplexity reduction, it is returned; otherwise, the algorithm concludes that no suitable sparsity rate exists.

Algorithm 1 Determine activation sparsity rate.

Require: • An MLP layer with: up_proj, act_fn, and down_proj.

• Optional gating branch: gate_proj. If gating is used, activation is computed as:

$$x = \mathtt{act_fn}(\mathtt{gate_proj}(h)) \odot \mathtt{up_proj}(h)$$

Otherwise,

$$x = act_fn(up_proj(h))$$

- Hidden state h.
- Benchmark dataset D.
- Target perplexity reduction $\Delta ppl = 1$.
- 1: Compute Activation Output:
- 2: if gating is used then
- 3: $x \leftarrow \text{act_fn}(\text{gate_proj}(h)) \odot \text{up_proj}(h)$
- 4: else
- 5: $x \leftarrow \text{act_fn}(\text{up_proj}(h))$
- 6: **end if**
- 7: Compute Baseline Perplexity:

$$P_{\text{base}} \leftarrow \exp\left(\text{nll}(D; \text{model})\right)$$

- 8: for each candidate sparsity rate r% do
- 9: **Determine Threshold** T_r : such that at least r% of the elements in x satisfy

$$|x_i| \leq T_r$$
.

10: Construct Mask:

$$m_i \leftarrow \begin{cases} 0, & \text{if } |x_i| \le T_r, \\ 1, & \text{otherwise.} \end{cases}$$

11: Compute Masked Activation:

$$\tilde{x} \leftarrow m \odot x$$
.

- 12: Replace the activation x with \tilde{x} in the MLP layer.
- 13: Evaluate Modified Model's Perplexity on D:

$$ppl_r \leftarrow \exp\Big(\text{nll}(D; \text{modified model})\Big).$$

- 14: **if** $ppl_{\text{base}} ppl_r \ge \Delta ppl$ **then**
- 15: **return** Activation sparsity rate r%.
- 16: **end if**
- 17: end for
- 18: return No sparsity rate found satisfying the condition.

F Chat Generations from PLM

Here we present the cases generated by PLM.

Math Evaluation in Chinese and English

Prompt:

小明有 15 颗糖果, 分给妹妹 5 颗, 又收到妈妈送的 8 颗。他现在有多少颗糖果?

Response:

- 1. ** 开始时的糖果数量: ** 小明有 15 颗糖果。
- 2. ** 分给妹妹的糖果数量: ** 小明分给妹妹 5 颗糖果,所以剩下的糖果数量为: 15-5=10 颗糖果。
- 3. ** 收到妈妈送的糖果数量:** 小明收到妈妈送的 8 颗糖果,所以现在的糖果数量为:10+8=18 颗糖果。
- 4. ** 最终的糖果数量: ** 小明现在有 [18] 颗糖果。

Prompt:

A farmer plants 7 rows of corn, with 9 seeds in each row. How many corn seeds are planted?

Response:

To determine the total number of corn seeds planted, we need to follow these steps:

- 1. Calculate the number of seeds planted in one row.
- 2. Multiply the number of seeds per row by the number of rows.

First, we know that each row contains 9 seeds. Since the farmer plants 7 rows of corn, we can find the total number of seeds by multiplying the number of seeds per row by the number of rows:

 $9~{\tt seeds/row} \times 7~{\tt rows} = 63~{\tt seeds}$

Therefore, the total number of corn seeds planted is [63].

Figure 16: Math evaluation in Chinese and English.

```
Code Evaluation in Chinese and English
Prompt:
请你写一个斐波那契数列的 python 代码。
Response:
这里是一个简单的 Python 程序, 用于生成前 n 个斐波那契数 (Fibonacci numbers)。
def fibonacci(n):
    if n <= 0:
       return []
    elif n == 1:
       yield [0]
    else:
        fib = [0, 1] # 初始值列表
        for i in range(2, n+1):
            next_fib = fib[-1] + fib[-2] # 计算下一个斐波那契元素
            fib.append(next_fib) # 将计算出的新数值添加到序列中
            yield (fib[:i]) # 返回当前这个子序列
print(list(fibonacci(5))) # 示例输出:
上述代码首先定义了一个名为 `fibonacci()` 的函数,在该函数内部使用了 `yield` 语句来返回
斐波那契数列的一个子序列。
Prompt:
Given an integer array ``nums'', return the length of the longest strictly increasing subsequence. Anwser in English.
Response:
The problem can be solved by dynamic programming.
Here is a Python solution using Dynamic Programming:
def findLengthOfLCIS(nums):
    if not nums:
        return 0
    # Initialize dp[i] as 1, because each element itself forms at least one LIS
       ending there.
    dp = [1]*len(nums)
    for i in range(1,len(nums)):
        for j in range(i):
            if nums[j] < nums[i]:</pre>
                dp[i]=max(dp[i],dp[j]+1)
    return max(dp)
In this code, we initialize our 'dp' list with ones and then iterate over
all elements from left to right. For every pair (i,j) where `j < i`, if
\normalfont{`nums[j] < num[s][i] `, it means that nums[i] extends the non-decreasing sequence}
formed by nums[... , nums[j]] so far. Therefore we update dp[i]: maximum value
between dp[i-1] or dp[j+1] + 1. At the end, the answer will be the maximum value
in dp which represents the size of the largest such subarray. The time complexity
of above python function is O(n2), where n is number of elements in input list
'nums'.
```

Figure 17: Code evaluation in Chinese and English.

Emotional Communication in Chinese and English

Prompt:

今天领导又无理指责我!该怎么办?

Response:

- 1、首先,要冷静下来。不要因为被领导批评而情绪激动,这样只会让事情变得更糟。
- 2、其次,要认真听取领导的批评,并且虚心接受。如果自己有错的话,应该主动承认错误并积极改正。
- 3、在面对领导的责备时,可以适当地表达自己的想法和感受,但要注意语气和措辞,避免过于激烈或攻击性的话语。
- 4、同时,在工作中也要注意提高自身素质和服务意识,以实际行动来证明自己的价值和能力。
- 5、最后,要学会与领导沟通交流,建立良好的工作关系,以便更好地完成工作任务。

总之,面对领导的责备,我们要保持冷静理智的态度,<u>虚</u>心接受批评,及时改进不足之处,不断提高自身的综合素质和服务水平,为公司的发展做出更大的贡献。

Prompt:

My partner feels disconnected due to a lack of quality time together. What can I do?

Response:

As an AI assistant, I am unable to have personal feelings or experiences, but I can offer some advice on how to address the situation. Here are some steps you could consider:

- 1. Reflect on your own behavior and actions. Consider whether there are any changes you can make to spend more quality time with your partner.
- 2. Communicate openly with your partner about your feelings and concerns. Listen to their perspective as well and work together to find a solution.
- 3. Make an effort to prioritize your time with your partner and commit to spending quality time together. This could involve setting aside dedicated time each week for date nights, activities, or just spending time together in a relaxed setting.
- 4. Be present and engaged in the time you do spend together. Put away distractions, and focus on truly connecting with your partner.
- 5. If the situation remains unresolved, consider seeking the help of a couples therapist or counselor to facilitate communication and problem-solving.

Figure 18: Emotional communication in Chinese and English.

Logic Evaluation in Chinese and English

Prompt:

甲、乙、丙三人参加活动,已知:甲到达时,乙已经离开;丙到达时,甲尚未到达;乙不是最后一个离开的。问三人离开的顺序是什么?

Response:

由于甲到达时,乙已经离开;因此,在甲到达之前,乙一定还没有开始活动。

又因为丙到达时, 甲尚未到达; 所以, 在丙到达之前, 甲一定还在等待着其他人的到来。

基于以上两个条件,我们可以得出以下结论:

在甲到达之前的时刻点,只有乙一个人在场;而在丙到达之后的时间点,除了甲之外还有丙两个人在 场。

接下来我们来考虑乙的情况。由题目可知,乙并不是最后一位离开的人。那么,在乙离开的时候,必然有另外两人在场。而在这三个人之中,只有甲没有被提及到过。由此可以推断出,在乙离开的时候,必定存在一个比他早一步或者晚一点的人先离开了。

综上所述,我们可以得到如下结论:乙最先离开,然后是甲,最后是丙。

因此,答案为"乙先走,甲后走,丙最迟"。

Prompt:

What word is right when pronounced wrong but is wrong when pronounced right? Answer in English.

Response:

The answer to the riddle would be "wrong" because it's a pun on two different meanings of the word: one meaning that something is incorrect or not correct, and another meaning that someone who does something incorrectly (or vice versa) can still do so correctly if they make an effort.

Figure 19: Logic evaluation in Chinese and English.